

Chapter 2

Mechanics of the Wheel with Tire



All road vehicles have wheels and almost all of them have *wheels with pneumatic tires*. Wheels have been around for many centuries, but only with the invention, and enhancement, of the pneumatic tire it has been possible to conceive fast and comfortable road vehicles [5].

The main features of any tire are its *flexibility* and *low mass*, which allow for the contact with the road to be maintained even on uneven surfaces. Moreover, the rubber ensures *high grip*. These features arise from the highly composite structure of tires: a carcass of flexible, yet almost inextensible cords encased in a matrix of soft rubber, all inflated with air.¹ Provided the (flexible) tire is properly inflated, it can exchange along the bead relevant actions with the (rigid) rim. Traction, braking, steering and load support are the net result.

It should be appreciated that the effect of air pressure is to increase the structural stiffness of the tire, not to support directly the rim. How a tire carries a vertical load F_z if properly inflated is explained in Fig. 2.1.² In the lower part the radial cords encased in the sidewalls undergo a reduction of tension because they no longer have to balance the air pressure p_a acting on the contact patch [10, p. 279]. The net result is that the total upward pull of the cords on the bead exceeds that of the downward pull by an amount equal to the vertical load F_z [26, p. 161]. A very clear explanation can also be found in [31].

¹ Only in competitions it is worthwhile to employ special (and secret) gas mixtures instead of air. The use of nitrogen, as often recommended, is in fact almost equivalent to air [18], except for the cost.

² As pointed out by Jon W. Mooney in his review, in Noise Control Engineering Journal, Vol. 62, 2014, the explanation and the figure provided in the first edition of this book were *not correct*. A similar (incorrect) explanation has appeared in [9, Fig. 1.19], published in 2017.

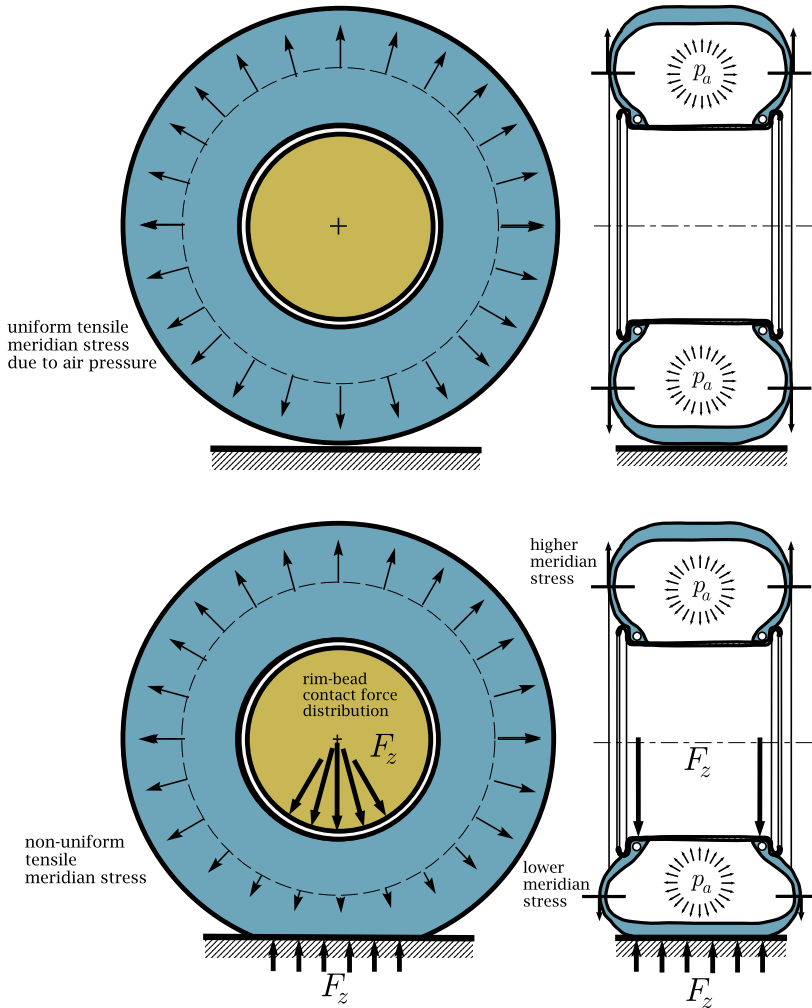


Fig. 2.1 How a tire carries a vertical load if properly inflated

The *contact patch*, or footprint, of the tire is the area of the tread in contact with the road. This is the area that transmits forces between the tire and the road via pressure and friction. To truly understand some of the peculiarities of tire mechanics it is necessary to get some insights on what happens in the contact patch.

Handling of road vehicles is strongly affected by the mechanical behavior of the wheels with tire, that is by the *relationship* between the *kinematics* of the rigid rim and the *force* exerted by the road. This chapter is indeed devoted to the analysis of experimental tests. The development of simple, yet significant, tire models is done in Chap. 11.

2.1 The Tire as a Vehicle Component

A wheel with tire is barely a wheel, in the sense that it behaves quite differently from a rigid wheel.³ This is a key point to really understand the mechanics of wheels with tires. For instance, a rigid wheel touches the (flat) road at one point C , whereas a tire has a fairly large contact patch. Pure rolling of a rigid wheel is a clear kinematic concept [17], but, without further discussion, it is not obvious whether an analogous concept is even meaningful for a tire. Therefore, we have to be careful in stating as clearly as possible the concepts needed to study the mechanics of wheels with tire.

Moreover, the analysis of tire mechanics will be developed with no direct reference to the dynamics of the vehicle. This may sound a bit odd, but it is not. The goal here is to describe the *relationship* between the *motion* and *position* of the rim and the *force* exchanged with the road through the *contact patch*:

$$\text{rim kinematics} \quad \Longleftrightarrow \quad \text{force and moment}$$

Once this description has been obtained and understood, then it can be employed as one of the fundamental components in the development of suitable models for vehicle dynamics, but this is the subject of other chapters.

Three basic components play an active role in tire mechanics:

1. the *rim*, which is assumed to be a rigid body;
2. the flexible *carcass* of the inflated tire;
3. the *contact patch* between the tire and the road.

2.2 Carcass Features

The tire carcass \mathcal{C} is a highly composite and complex structure. Here we look at the tire as a vehicle component [19] and therefore it suffices to say that the inflated carcass, with its flexible sidewalls, is moderately compliant in all directions (Figs. 2.1 and 2.2). The external belt is also flexible, but quite inextensible (Fig. 2.3). For instance, its circumferential length is not very much affected by the vertical load acting on the tire. The belt is covered with tread blocks whose elastic deformation and grip features highly affect the mechanical behavior of the wheel with tire [13–15].

Basically, the carcass can be seen as a nonlinear elastic structure with small hysteresis due to rate-dependent energy losses. It is assumed here that the carcass and the belt have negligible inertia, in the sense that the inertial effects are small in comparison with other causes of deformation. This is quite correct if the road is flat and the wheel motion is not “too fast”.

³ A rigid wheel is essentially an axisymmetric convex rigid surface. The typical rigid wheel is a toroid.

Fig. 2.2 Radial flexibility of the tire carcass [13]

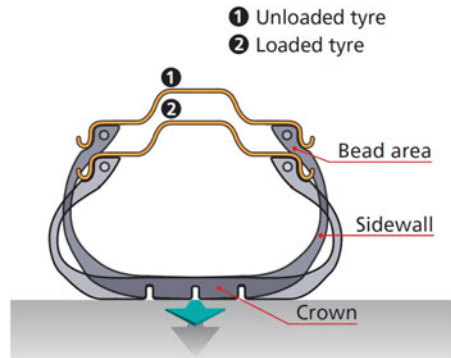


Fig. 2.3 Structure of a radial tire [13]



2.3 Contact Patch

Tires are made from rubber, that is elastomeric materials to which they owe a large part of their grip capacity [25]. Grip implies contact between two surfaces: one is the tire surface and the other is the road surface.

The contact patch (or footprint) \mathcal{P} is the region where the tire is in contact with the road surface. Most tires have a tread pattern, with lugs and voids, and hence the contact patch is the union of many small regions (Fig. 2.4). It should be emphasized that the shape and size of the contact patch, and also its position with respect to the rim, depend on the tire operating conditions.

Grip depends, among other things, on the *type* of road surface, its *roughness* and whether it is *wet or not*. More precisely, grip comes basically from road roughness effects and molecular adhesion.

Road roughness effects, also known as indentation, require small bumps measuring a few microns to a few millimeters (Fig. 2.5), which dig into the surface of the rubber. On the other hand, *molecular adhesion* necessitates direct contact between the rubber and the road surface, i.e. the road must be dry.




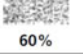

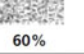
Percentage of contact with the road and pressure in the contact patch				
Inflation pressure	2 bars	 150 cm ²	8 bars	 500 cm ²
Rubber/void percentage	30 %		30 %	
Mean pressure in the contact patch	3 bars		11 bars	
Percentage of rubber in contact with the road (load bearing surface)	on very rough surfaces	on slightly rough surfaces	on very rough surfaces	on slightly rough surfaces
	 7%	 60%	 7%	 60%
Local pressure on rough spots (mean value)	43 bars	5 bars	157 bars	18 bars

Fig. 2.4 Typical contact patches with tread pattern (1 bar = 0.1 MPa = 14.5 psi) [13]

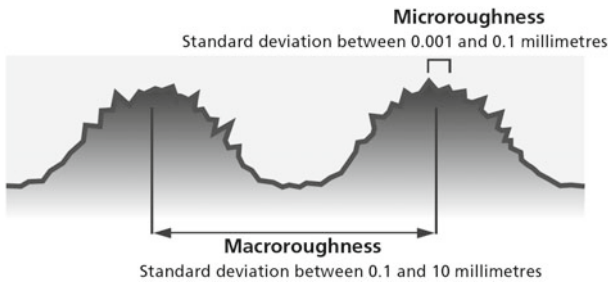


Fig. 2.5 Road roughness description [13]

Two main features of road surface geometry must be examined and assessed when considering tire grip, as shown in Fig. 2.5:

Macroroughness: this is the name given to the road surface texture when the distance between two consecutive rough spots is between 100 microns and 10 millimeters. This degree of roughness contributes to indentation, and to the drainage and storage of water. The load-bearing surface, which depends on road macroroughness, must also be considered since it determines local pressures in the contact patch.

Microroughness: this is the name given to the road surface texture when the distance between two consecutive rough spots is between 1 and 100 microns. It is this degree of roughness that is mainly responsible for tire grip via the road roughness effects. Microroughness is related to the surface roughness of the aggregates and sands used in the composition of the road surface.

In Fig. 2.6 the contact patch is schematically shown as a single region.

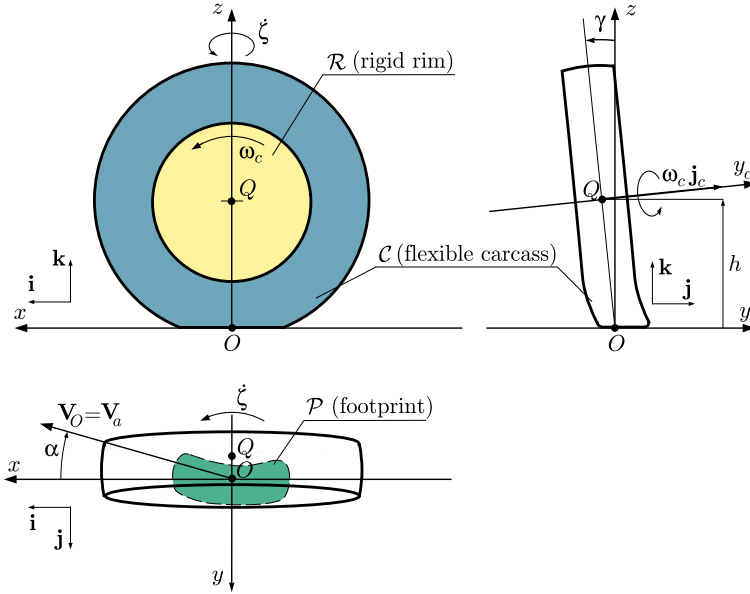


Fig. 2.6 Wheel with tire: nomenclature and reference system $\mathcal{S}_w = (x, y, z; O)$

2.4 Rim Position and Motion

For simplicity, the *road* is assumed to have a hard and *flat* surface, like a *geometric plane*. This is a good model for any road with high quality asphalt paving, since the texture of the road surface is not relevant for the definition of the rim kinematics (while it highly affects grip [13]).

The *rim* \mathcal{R} is assumed to be a *rigid body*, and hence, in principle, it has six degrees of freedom. However, only two degrees of freedom (instead of six) are really relevant for the rim *position* because the road is *flat* and the wheel rim is *axisymmetric*. Let Q be a point on the rim axis y_c (Fig. 2.6). Typically, although not strictly necessary, a sort of midpoint is taken. The *position* of the rim with respect to the flat road depends only on the *height* h of Q and on the *camber angle* γ (i.e., the inclination) of the rim axis y_c . More precisely, h is the distance of Q from the road plane and γ is the angle between the rim axis and the road plane.

In [32] and [22] the distance h is called loaded tire radius. In our opinion, the word “radius” may be misleading. There is no circle with radius h .

Now, we can address how to describe the rim velocity field.

The rim, being a rigid body, has a well defined angular velocity $\boldsymbol{\Omega}$. Therefore, the velocity of any point P of the (space moving with the) rim is given by the well known equation [12, p. 124]

$$\mathbf{V}_P = \mathbf{V}_Q + \boldsymbol{\Omega} \times \mathbf{QP} \quad (2.1)$$

where \mathbf{V}_Q is the velocity of Q and QP is the vector connecting Q to P . The three components of \mathbf{V}_Q and the three components of $\boldsymbol{\Omega}$ are, e.g., the *six* parameters which completely determine the rim *velocity* field.

2.4.1 Reference System

A moving reference system $\mathbf{S}_w = (x, y, z; O)$ is depicted in Fig. 2.6. It is defined in a fairly intuitive way. The y -axis is the intersection between a vertical plane containing the rim axis y_c and the road plane. The x -axis is given by the intersection of the road plane with a plane containing Q and normal to y_c . The intersection between axes x and y defines the origin O as a point on the road. The z -axis is vertical, that is perpendicular to the road, with the positive direction upward.⁴ The unit vectors marking the positive directions are $(\mathbf{i}, \mathbf{j}, \mathbf{k})$, as shown in Fig. 2.6.

An observation is in order here. The *directions* $(\mathbf{i}, \mathbf{j}, \mathbf{k})$ have a physical meaning, in the sense that they clearly mark some of the peculiar features of the rim with respect to the road. As a matter of fact, \mathbf{k} is perpendicular to the road, \mathbf{i} is perpendicular to both \mathbf{k} and the rim axis \mathbf{j}_c , \mathbf{j} follows accordingly. However, the *position* of the Cartesian axes (x, y, z) is arbitrary, since there is no physical reason to select a point as the origin O . This is an aspect whose implications are often underestimated.

The selected point O is often called *center of the footprint*, or center of the wheel.

2.4.2 Rim Kinematics

The moving reference system $\mathbf{S}_w = (x, y, z; O)$ allows a more precise description of the rim kinematics. On the other hand, a reference system $\mathbf{S}_f = (x_f, y_f, z_f; O_f)$ fixed to the road is not very useful in this context.

Let \mathbf{j}_c be the direction of the rim spindle axis y_c

$$\mathbf{j}_c = \cos \gamma \mathbf{j} + \sin \gamma \mathbf{k} \quad (2.2)$$

where the *camber angle* γ of Fig. 2.6 is positive. The total *rim angular velocity* $\boldsymbol{\Omega}$ is

$$\begin{aligned} \boldsymbol{\Omega} &= \dot{\gamma} \mathbf{i} + \dot{\theta} \mathbf{j}_c + \dot{\zeta} \mathbf{k} \\ &= \dot{\gamma} \mathbf{i} + \omega_c \mathbf{j}_c + \omega_z \mathbf{k} \\ &= \dot{\gamma} \mathbf{i} + \omega_c \cos \gamma \mathbf{j} + (\omega_c \sin \gamma + \omega_z) \mathbf{k} \\ &= \Omega_x \mathbf{i} + \Omega_y \mathbf{j} + \Omega_z \mathbf{k} \end{aligned} \quad (2.3)$$

⁴ \mathbf{S}_w is the system recommended by ISO (see, e.g., [20, Appendix 1])

where $\dot{\gamma}$ is the time derivative of the camber angle, $\omega_c = \dot{\theta}$ is the angular velocity of the rim about its spindle axis \mathbf{j}_c , and $\omega_z = \dot{\zeta}$ is the yaw rate, that is the angular velocity of the reference system \mathbf{S}_w about the vertical axis \mathbf{k} .

It is worth noting that there are *two* distinct contributions to the *spin velocity* $\Omega_z \mathbf{k}$ of the rim,⁵ a *camber* contribution $\omega_c \sin \gamma$ and a *yaw rate* contribution ω_z

$$\Omega_z = \omega_c \sin \gamma + \omega_z \quad (2.4)$$

Therefore, as will be shown in Fig. 2.19, the same value of Ω_z can be the result of different operating conditions for the tire, depending on the amount of the *camber angle* γ and of the *yaw rate* ω_z .

By definition, the position vector OQ is (Fig. 2.6)

$$OQ = h(-\tan \gamma \mathbf{j} + \mathbf{k}) \quad (2.5)$$

This expression can be differentiated with respect to time to obtain

$$\begin{aligned} \mathbf{V}_Q - \mathbf{V}_O &= \dot{h}(-\tan \gamma \mathbf{j} + \mathbf{k}) + h \left(\omega_z \tan \gamma \mathbf{i} - \frac{\dot{\gamma}}{\cos^2 \gamma} \mathbf{j} \right) \\ &= h \omega_z \tan \gamma \mathbf{i} - \left(\dot{h} \tan \gamma + h \frac{\dot{\gamma}}{\cos^2 \gamma} \right) \mathbf{j} + \dot{h} \mathbf{k} \end{aligned} \quad (2.6)$$

since $d\mathbf{j}/dt = -\omega_z \mathbf{i}$. Even in steady-state conditions, that is $\dot{h} = \dot{\gamma} = 0$, we have $\mathbf{V}_Q = \mathbf{V}_O + h \omega_z \tan \gamma \mathbf{i}$ and hence the velocities of points Q and O are not exactly the same, unless also $\gamma = 0$. The camber angle γ is usually very small in cars, but may be quite large in motorcycles (up to 60 deg).

The velocity $\mathbf{V}_o = \mathbf{V}_O$ of point O has, in general, longitudinal and lateral components (Fig. 2.6)⁶

$$\begin{aligned} \mathbf{V}_o &= V_{o_x} \mathbf{i} + V_{o_y} \mathbf{j} \\ &= V_{o_x} (\mathbf{i} - \tan \alpha \mathbf{j}) \end{aligned} \quad (2.7)$$

where α is the wheel *slip angle*.

As already stated, the selection of point O is *arbitrary*, although quite reasonable. Therefore, the velocities V_{o_x} and V_{o_y} do not have much of a physical meaning. A different choice for the point O would provide different values for the very same motion. However, a wheel with tire is expected to have longitudinal velocities much higher than lateral ones, that is $|\alpha| < 12^\circ$, as will be discussed with reference to Fig. 11.33.

Summing up, the position of the rigid rim \mathcal{R} with respect to the flat road is completely determined by the following six degrees of freedom:

$h(t)$ distance of point Q from the road (often, improperly, called loaded radius);

⁵ In the SAE terminology, it is $\omega_c \mathbf{j}_c$ that is called spin velocity [6, 16].

⁶ The two symbols \mathbf{V}_o and \mathbf{V}_O are equivalent. Using \mathbf{V}_o is just a matter of taste.

- $\gamma(t)$ camber angle;
- $\theta(t)$ rotation of the rim about its axis y_c ;
- $x_f(t)$ first coordinate of point O w.r.t. \mathbf{S}_f ;
- $y_f(t)$ second coordinate of point O w.r.t. \mathbf{S}_f ;
- $\zeta(t)$ yaw angle of the rim.

However, owing to the *circular* shape of rim and the *flatness* of the road, the kinematics of the rigid rim \mathcal{R} is also fully described by the following six functions of time:

- $h(t)$ distance of point Q from the road;
- $\gamma(t)$ camber angle;
- $\omega_c(t)$ angular velocity of the rim about its axis y_c ;
- $V_{o_x}(t)$ longitudinal speed of O ;
- $V_{o_y}(t)$ lateral speed of O ;
- $\omega_z(t)$ yaw rate of the moving reference system \mathbf{S}_w .

The rim is in steady-state conditions if all these six quantities are constant in time. However, this is not sufficient for the wheel with tire to be in a stationary state. The flexible carcass and tire treads could still be under transient conditions.

Now, there is an observation whose practical effects are very important. If we are interested only in the truly kinematic (geometric) features of the rim motion, we can drop the number of required functions from six to five:

$$h, \quad \gamma, \quad \frac{V_{o_x}}{\omega_c}, \quad \frac{V_{o_y}}{\omega_c}, \quad \frac{\omega_z}{\omega_c} \quad (2.8)$$

Essentially, we are looking at the relative values of speeds, as if their magnitude were of no relevance at all. This is what is commonly done in vehicle dynamics, as we will see soon. Again, we emphasize that a vehicle engineer should be aware of what he/she is doing.

2.5 Footprint Force

As well known (see, e.g., [27]), any set of forces or distributed loads is statically equivalent to a force–couple system at a given (arbitrary) point O . Therefore, regardless of the degree of roughness of the road, the distributed normal and tangential loads in the footprint yield a resultant force \mathbf{F} and a resultant couple vector \mathbf{M}_O

$$\begin{aligned} \mathbf{F} &= F_x \mathbf{i} + F_y \mathbf{j} + F_z \mathbf{k} \\ \mathbf{M}_O &= M_x \mathbf{i} + M_y \mathbf{j} + M_z \mathbf{k} \end{aligned} \quad (2.9)$$

The resultant couple \mathbf{M}_O is simply the moment about the point O , but any other point could be selected. Therefore it has no particular physical meaning. However,

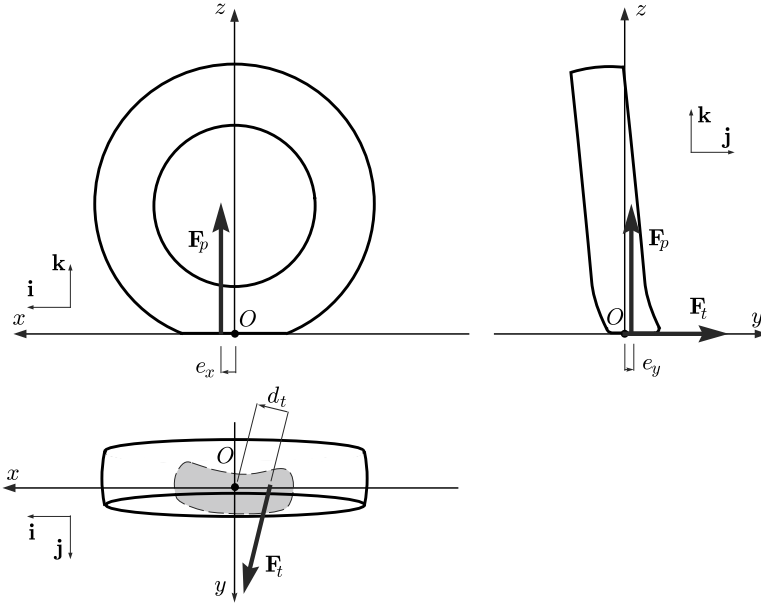


Fig. 2.7 Forces acting on the tire from the road

if O is somewhere within the footprint, the magnitude $|\mathbf{M}_O|$ is expected to be quite “small” for the wheel with tire to resemble a rigid wheel.

Traditionally, the components of \mathbf{F} and \mathbf{M}_O have the following names:

F_x longitudinal force ($F_x < 0$ when braking);

F_y lateral force;

F_z vertical load or normal force;

M_x overturning moment;

M_y rolling resistance moment;

M_z self-aligning torque, called vertical moment here.

The names of the force components simply reaffirm their directions with respect to the chosen reference system \mathbf{S}_w , and hence with respect to the rim. On the other hand, the names of the moment components, which would suggest a physical interpretation, are all quite questionable. Their values depend on the arbitrarily selected point O , and hence are arbitrary by definition.

For instance, let us discuss the name “self-aligning torque” of M_z , with reference to Fig. 2.7 and Eq. (2.11). The typical explanation for the name is that “ M_z produces a restoring moment on the tire to realign the direction of travel with the direction of heading”, which, more precisely, means that M_z and the slip angle α are both clockwise or both counterclockwise. But the sign and magnitude of M_z depend on the position of O , which could be anywhere! The selected origin O has nothing

special, nothing at all. Therefore, the very same physical phenomenon, like in Fig. 2.7, may be described with O anywhere and hence by any value of M_z . The inescapable conclusion is that the name “self-aligning torque” is totally meaningless and even misleading.⁷ For these reasons, here we prefer to call M_z the *vertical moment*. Similar considerations apply to M_x and M_y .

It is a classical result that any set of forces and couples in space, like $(\mathbf{F}, \mathbf{M}_O)$, is statically equivalent to a unique wrench [27]. However, in tire mechanics it is more convenient, although not mandatory, to represent the force–couple system $(\mathbf{F}, \mathbf{M}_O)$ by *two* properly located *perpendicular forces* (Fig. 2.7): a vertical force $\mathbf{F}_p = F_z \mathbf{k}$ having the line of action passing through the point with coordinates $(e_x, e_y, 0)$ such that

$$M_x = F_z e_y \quad \text{and} \quad M_y = -F_z e_x \quad (2.10)$$

and a tangential force $\mathbf{F}_t = F_x \mathbf{i} + F_y \mathbf{j}$ lying in the xy -plane and having the line of action with distance $|d_t|$ from O , properly located according to the sign of d_t

$$M_z = \sqrt{F_x^2 + F_y^2} d_t = |\mathbf{F}_t| d_t \quad (2.11)$$

We remark that the two “displaced” forces \mathbf{F}_p and \mathbf{F}_t (Fig. 2.7) are completely equivalent to \mathbf{F} and \mathbf{M}_O .

These forces are transferred to the rigid rim (apart for a small fraction due to the inertia and weight of the tire carcass and belt). Indeed, the equivalence of the distributed loads in the contact patch to concentrated forces and/or couples makes sense precisely because the rim is a rigid body.

2.5.1 Perfectly Flat Road Surface

To perform some further mathematical investigations, it is necessary to completely discard road roughness (Fig. 2.5) and to assume that the road surface in the contact patch is *perfectly flat*, exactly like a geometric plane (Figs. 2.6 and 2.7).⁸ This is a fairly unrealistic assumption whose implications should not be underestimated.

Owing to the assumed flatness of the contact patch \mathcal{P} , we have that the *pressure* $p(x, y) \mathbf{k}$, by definition normal to the surface, is always vertical and hence forms a *parallel* distributed load. Moreover, the flatness of \mathcal{P} implies that the *tangential stress* $\mathbf{t}(x, y) = t_x \mathbf{i} + t_y \mathbf{j}$ forms a *planar* distributed load. Parallel and planar distributed loads share the common feature that the resultant force and the resultant couple vector are perpendicular to each other, and therefore each force–couple system at O can be

⁷ What is relevant in vehicle dynamics is the moment of $(\mathbf{F}, \mathbf{M}_O)$ with respect to the steering axis of the wheel. But this is another story (Fig. 3.1).

⁸ More precisely, it is necessary to have a mathematical description of the shape of the road surface in the contact patch. The plane just happens to be the simplest.

further reduced to a *single* resultant force applied along the *line of action* (in general not passing through O). A few formulas should clarify the matter.

The resultant *vertical* force \mathbf{F}_p and horizontal couple \mathbf{M}_p^O of the distributed pressure $p(x, y)$ are given by

$$\begin{aligned}\mathbf{F}_p &= F_z \mathbf{k} = \mathbf{k} \iint_{\mathcal{P}} p(x, y) dx dy \\ \mathbf{M}_p^O &= M_x \mathbf{i} + M_y \mathbf{j} = \iint_{\mathcal{P}} (x \mathbf{i} + y \mathbf{j}) \times \mathbf{k} p(x, y) dx dy\end{aligned}\quad (2.12)$$

where

$$M_x = \iint_{\mathcal{P}} y p(x, y) dx dy = F_z e_y, \quad M_y = - \iint_{\mathcal{P}} x p(x, y) dx dy = -F_z e_x \quad (2.13)$$

As expected, \mathbf{F}_p and \mathbf{M}_p^O are perpendicular. As shown in (2.13), the force–couple resultant $(\mathbf{F}_p, \mathbf{M}_p^O)$ can be reduced to a single force \mathbf{F}_p having a vertical line of action passing through the point with coordinates $(e_x, e_y, 0)$, as shown in Fig. 2.7.

The resultant *tangential* force \mathbf{F}_t and vertical couple \mathbf{M}_t^O of the distributed tangential (grip) stress $\mathbf{t}(x, y) = t_x \mathbf{i} + t_y \mathbf{j}$ are given by

$$\begin{aligned}\mathbf{F}_t &= F_x \mathbf{i} + F_y \mathbf{j} = \iint_{\mathcal{P}} (t_x(x, y) \mathbf{i} + t_y(x, y) \mathbf{j}) dx dy \\ \mathbf{M}_t^O &= M_z \mathbf{k} = \iint_{\mathcal{P}} (x \mathbf{i} + y \mathbf{j}) \times (t_x(x, y) \mathbf{i} + t_y(x, y) \mathbf{j}) dx dy \\ &= \mathbf{k} \iint_{\mathcal{P}} (x t_y(x, y) - y t_x(x, y)) dx dy = \mathbf{k} d_t \sqrt{F_x^2 + F_y^2}\end{aligned}\quad (2.14)$$

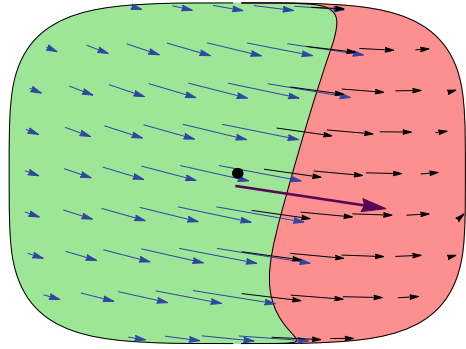
where

$$F_x = \iint_{\mathcal{P}} t_x(x, y) dx dy, \quad F_y = \iint_{\mathcal{P}} t_y(x, y) dx dy \quad (2.15)$$

$$d_t = \frac{M_z}{\sqrt{F_x^2 + F_y^2}} \quad (2.16)$$

Also in this case \mathbf{F}_t and \mathbf{M}_t^O are perpendicular. As shown in (2.14), the force–couple resultant $(\mathbf{F}_t, \mathbf{M}_t^O)$ can be reduced to a tangential force \mathbf{F}_t , lying in the xy -plane and having a line of action with distance $|d_t|$ from O (properly located according to the sign of d_t), as shown in Fig. 2.7.

Fig. 2.8 Example of distributed tangential stress in the contact patch, along with the corresponding resultant tangential force \mathbf{F}_t . Reference system as in Fig. 2.7 (bottom)



Obviously, the more general (2.9) still holds

$$\begin{aligned}\mathbf{F} &= \mathbf{F}_p + \mathbf{F}_t \\ \mathbf{M}_O &= \mathbf{M}_p^O + \mathbf{M}_t^O\end{aligned}\quad (2.17)$$

An example of distributed tangential stress is shown in Fig. 2.8. It was obtained by means of the tire brush model, a topic developed in Chap. 11.

2.6 Global Mechanical Behavior

The analysis developed so far provides the tools for quite a precise description of the global mechanical behavior of a *real* wheel with tire interacting with a road. More precisely, as already stated on Sect. 2.1, we are interested in the *relationship* between the *motion* and *position* of the rim and the *force* exchanged with the road in the *contact patch*.

We assume as given, and constant in time, both the wheel with tire (including its inflation pressure and temperature field) and the road type (including its roughness). Therefore we assume all grip features as given and constant in time.

2.6.1 Tire Transient Behavior

Knowing the mechanical behavior means knowing the relationships between the six kinematical parameters $(h, \gamma, \omega_c, V_{ox}, V_{oy}, \omega_z)$ that fully characterize the position and the motion of the rigid rim and the force–couple resultant $(\mathbf{F}, \mathbf{M}_O)$. We recall that the inertial effects of the carcass are assumed to be negligible.

Owing mostly to the flexibility of the tire structure, these relationships are of differential type, that is there exist *differential* equations

$$\begin{aligned} \mathbf{f}(\dot{\mathbf{F}}, \mathbf{F}, h, \gamma, \omega_c, V_{ox}, V_{oy}, \omega_z) &= \mathbf{0} \\ \mathbf{g}(\dot{\mathbf{M}}_O, \mathbf{M}_O, h, \gamma, \omega_c, V_{ox}, V_{oy}, \omega_z) &= \mathbf{0} \end{aligned} \quad (2.18)$$

In general, differential equations of higher order may be needed.

The identification of these differential equations by means solely of experimental tests is a formidable task. The point here is not to find them, but to appreciate that the transient behavior of a wheel with tire does indeed obey differential equations, maybe like in (2.18). Which also implies that *initial conditions* have to be included and the values of $(\mathbf{F}, \mathbf{M}_O)$ at time t depend on time history.

In Chap. 11, suitable models will be developed that allow to partially identify (2.18).

2.6.2 Tire Steady-State Behavior

If all features are constant (or, at least, slowly varying) in time, the overall system is in steady-state conditions. Mathematically, it means that there exist, instead of (2.18), the following *algebraic* functions

$$\begin{aligned} \mathbf{F} &= \bar{\mathbf{F}}(h, \gamma, \omega_c, V_{ox}, V_{oy}, \omega_z) \\ \mathbf{M}_O &= \bar{\mathbf{M}}_O(h, \gamma, \omega_c, V_{ox}, V_{oy}, \omega_z) \end{aligned} \quad (2.19)$$

which relate the rim position and steady-state motion to the force and moment acting on the tire from the footprint. In other words, given the steady-state kinematics of the rim, we know the (constant in time) forces and couples (but not viceversa).⁹

The algebraic functions in (2.19) are, by definition, the equilibrium states of the differential equations (2.18)

$$\begin{aligned} \mathbf{f}(\mathbf{0}, \bar{\mathbf{F}}, h, \gamma, \omega_c, V_{ox}, V_{oy}, \omega_z) &= \mathbf{0} \\ \mathbf{g}(\mathbf{0}, \bar{\mathbf{M}}_O, h, \gamma, \omega_c, V_{ox}, V_{oy}, \omega_z) &= \mathbf{0} \end{aligned} \quad (2.20)$$

Equations (2.19) can be split according to (2.17)

$$\begin{aligned} \mathbf{F}_p &= F_z \mathbf{k} = \bar{\mathbf{F}}_p(h, \gamma, \omega_c, V_{ox}, V_{oy}, \omega_z) \\ \mathbf{F}_t &= F_x \mathbf{i} + F_y \mathbf{j} = \bar{\mathbf{F}}_t(h, \gamma, \omega_c, V_{ox}, V_{oy}, \omega_z) \\ \mathbf{M}_p^O &= M_x \mathbf{i} + M_y \mathbf{j} = \bar{\mathbf{M}}_p^O(h, \gamma, \omega_c, V_{ox}, V_{oy}, \omega_z) \\ \mathbf{M}_t^O &= M_z \mathbf{k} = \bar{\mathbf{M}}_t^O(h, \gamma, \omega_c, V_{ox}, V_{oy}, \omega_z) \end{aligned} \quad (2.21)$$

⁹ We remark that, as discussed in Chap. 11, steady-state kinematics of the rim does not necessarily implies steady-state behavior of the tire.

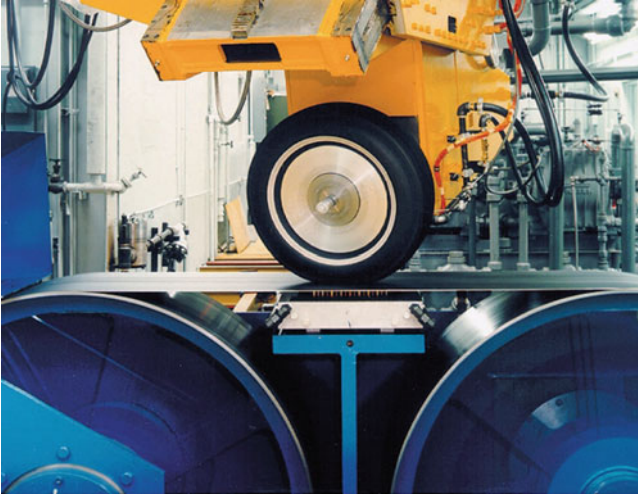


Fig. 2.9 Flat roadway testing machine (Calspan's Tire Research Facility)

2.6.3 Simplifications Based on Tire Tests

Typical *tire tests* (like those in Figs. 2.9 and 2.10) are aimed at investigating some aspects of these functions. It arises that the pressure-dependent forces and torques can be simplified drastically, since they are functions of h and γ only

$$\begin{aligned}\mathbf{F}_p &= F_z(h, \gamma) \mathbf{k} \\ \mathbf{M}_p^O &= M_x(h, \gamma) \mathbf{i} + M_y(h, \gamma) \mathbf{j}\end{aligned}\tag{2.22}$$

Actually, quite often the *vertical load* F_z takes the place of h as an independent variable, as discussed in Sect. 2.9. This is common practice, although it appears to be rather questionable in a neat approach to the analysis of tire mechanics. As already stated, a clearer picture arises if we follow the approach “impose the whole kinematics of the rim, measure all the forces in the contact patch” [20, p. 62].

2.6.3.1 Speed Independence (Maybe)

Moreover, tire tests suggest that the *grip force* $\mathbf{F}_t = F_x \mathbf{i} + F_y \mathbf{j}$ and moment $\mathbf{M}_t^O = M_z \mathbf{k}$ are *almost speed-independent*, if ω_c is not too high. Essentially, it means that

$$\begin{aligned}F_x &= \bar{F}_x(h, \gamma, \omega_c, V_{o_x}, V_{o_y}, \omega_z) \\ F_y &= \bar{F}_y(h, \gamma, \omega_c, V_{o_x}, V_{o_y}, \omega_z) \\ M_z &= \bar{M}_z(h, \gamma, \omega_c, V_{o_x}, V_{o_y}, \omega_z)\end{aligned}\tag{2.23}$$

Fig. 2.10 Drum testing machine [13]



can be replaced by the following functions of only *five* variables, as anticipated in (2.8):

$$\begin{aligned}
 F_x &= \tilde{F}_x \left(h, \gamma, \frac{V_{ox}}{\omega_c}, \frac{V_{oy}}{\omega_c}, \frac{\omega_z}{\omega_c} \right) \\
 F_y &= \tilde{F}_y \left(h, \gamma, \frac{V_{ox}}{\omega_c}, \frac{V_{oy}}{\omega_c}, \frac{\omega_z}{\omega_c} \right) \\
 M_z &= \tilde{M}_z \left(h, \gamma, \frac{V_{ox}}{\omega_c}, \frac{V_{oy}}{\omega_c}, \frac{\omega_z}{\omega_c} \right)
 \end{aligned} \tag{2.24}$$

In other words, we assume that the grip-dependent forces and moments depend on the *geometrical* features of the rim motion (i.e., the trajectories), and not on how fast the motion develops in time. Therefore, we are discarding all inertial effects and any influence of speed on the phenomena related to grip. Of course, this may not be true at very high speeds, like in competitions.

Actually, as will be discussed in Sect. 2.9, it is convenient to employ the *tire slips* as independent kinematic variables. Therefore, (2.24) is usually replaced by (2.79). But to do that we need first to define the *pure rolling* condition for tires, as done in (2.25), (2.26), and (2.27).

2.7 Definition of Pure Rolling for Tires

Pure rolling, in case of *rigid* bodies in *point contact*, requires two kinematical conditions to be fulfilled: *no sliding* and *no mutual spin*. However, the term pure rolling is somehow ambiguous, since absence of sliding does not exclude the transmission of a tangential force, lower in magnitude than the limiting friction. In [10, p. 242],

the terms *free rolling* and *tractive rolling* are used therefore to describe pure rolling of rigid bodies in which the tangential force is zero and non-zero, respectively.

These concepts and results are not, however, immediately applicable for the definition of pure rolling of a wheel with tire. As a matter of fact, there are no rigid surfaces in contact and the footprint is certainly not a point (Fig. 2.4). Therefore, even if it is customary to speak of pure rolling of a wheel with tire, it should be clear that it is a *different concept* than pure rolling between rigid bodies.

A reasonable definition of *pure rolling* for a wheel with tire, in steady-state conditions¹⁰ and moving on a flat surface, is that the grip actions \mathbf{t} have no *global* effect, that is

$$F_x = 0 \quad (2.25)$$

$$F_y = 0 \quad (2.26)$$

$$M_z = 0 \quad (2.27)$$

These equations do not imply that the local tangential stresses \mathbf{t} in the contact patch are everywhere equal to zero, but only that their force–couple resultant is zero (cf. (2.14) and see Fig. 11.52). Therefore, the road applies to the wheel only a vertical force $\mathbf{F}_p = F_z \mathbf{k}$ and a horizontal moment $\mathbf{M}_p^O = M_x \mathbf{i} + M_y \mathbf{j} \simeq M_y \mathbf{j}$.

Therefore, in our analysis, pure rolling of a wheel with tire means *torque rolling*. However, owing to the small values of the rolling resistance coefficient f_r (defined in Sect. 2.13), there is not much quantitative difference between torque rolling and tractive rolling for a wheel with tire.

The goal now is to find the *kinematical conditions* to be *imposed* to the rim to fulfill Eqs. (2.25)–(2.27), that is to have the just defined pure rolling conditions. In general, the six parameters in Eqs. (2.21) should be considered. However, it is more common to assume that *five* parameters suffice, like in (2.24) (as already discussed, it is less general, but simpler, to assume that the speed is not relevant)

$$\tilde{F}_x \left(h, \gamma, \frac{V_{ox}}{\omega_c}, \frac{V_{oy}}{\omega_c}, \frac{\omega_z}{\omega_c} \right) = 0 \quad (2.28)$$

$$\tilde{F}_y \left(h, \gamma, \frac{V_{ox}}{\omega_c}, \frac{V_{oy}}{\omega_c}, \frac{\omega_z}{\omega_c} \right) = 0 \quad (2.29)$$

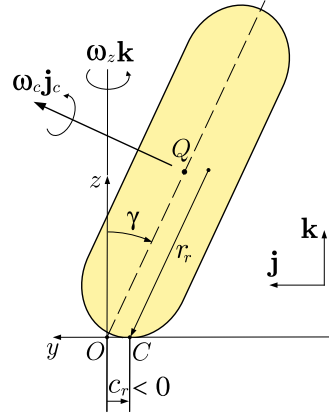
$$\tilde{M}_z \left(h, \gamma, \frac{V_{ox}}{\omega_c}, \frac{V_{oy}}{\omega_c}, \frac{\omega_z}{\omega_c} \right) = 0 \quad (2.30)$$

2.7.1 Zero Longitudinal Force (Rolling Radius)

First, let us consider Eq. (2.28) alone

¹⁰ We have basically a steady-state behavior even if the operating conditions do not change “too fast”.

Fig. 2.11 Longitudinal pure rolling of a cambered wheel. Definition of $c_r < 0$ and of point C



$$\tilde{F}_x \left(h, \gamma, \frac{V_{ox}}{\omega_c}, \frac{V_{oy}}{\omega_c}, \frac{\omega_z}{\omega_c} \right) = 0 \quad (2.31)$$

which means that $F_x = 0$ if¹¹

$$\frac{V_{ox}^r}{\omega_c} = f_x \left(h, \gamma, \frac{V_{oy}}{\omega_c}, \frac{\omega_z}{\omega_c} \right) \quad (2.32)$$

Under many circumstances, there is experimental evidence that the relation above almost does not depend on V_{oy} . Moreover, it can be recast in the following, more explicit form

$$\frac{V_{ox}^r}{\omega_c} = r_r(h, \gamma) + \frac{\omega_z}{\omega_c} c_r(h, \gamma) \quad (2.33)$$

that is

$$V_{ox}^r = \omega_c r_r(h, \gamma) + \omega_z c_r(h, \gamma) \quad (2.34)$$

where c_r is a (short) signed length, as shown in Fig. 2.11. This equation means that there exists a *special point* C of the y -axis such that

$$OC = c_r(h, \gamma) \mathbf{j} \quad (2.35)$$

Like O , also point C belongs to the moving reference system \mathbf{S}_w .

Therefore, (2.33) can be rearranged to get

$$V_{c_x}^r(\omega_c, h, \gamma) = \omega_c r_r(h, \gamma) = V_{ox}^r - \omega_z c_r(h, \gamma) \quad (2.36)$$

¹¹ As a general rule, a subscript or a superscript r means “pure rolling”.

This is quite a remarkable result and clarifies the role of point C : the condition $F_x = 0$ requires point C to have a longitudinal velocity $V_{c_x}^r = \omega_c r_r(h, \gamma)$, regardless of the value of the yaw rate ω_z .

The function $r_r(h, \gamma)$ in (2.33) can be seen as a sort of longitudinal *rolling radius* [30, p. 18], although this name would be really meaningful only for a rigid wheel. In [22, p. 3] r_r is called *effective rolling radius*.

Point C would be the point of contact in case of a rigid wheel (Fig. 2.11). For a wheel with tire, we can call C the *point of virtual contact*.

If $\gamma = 0$, the origin O of the reference system \mathbf{S}_w (Fig. 2.6) coincides with C . That is

$$c_r(h, 0) = 0 \quad (2.37)$$

and equations become much simpler.

The value of $r_r(h, \gamma)$ for given (h, γ) can be obtained by means of the usual indoor testing machines (Figs. 2.9 and 2.10) with $\omega_z = 0$. In most practical cases, particularly for radial tires, the rolling radius is quite insensitive to (reasonable) variations of h [22, p. 461]. Therefore

$$r_r(h, \gamma) \simeq r_r(\gamma) \quad (2.38)$$

Moreover, car tires operate at low values of γ and hence have almost constant r_r . This is not true for motorcycle tires.

An additional, more difficult, test with $\omega_z \neq 0$ is required to obtain also $c_r(h, \gamma)$ and hence the variable position of the point of virtual contact C with respect to O . Only for large values of the camber angle γ , that is for motorcycle tires, the distance $|c_r|$ can reach a few centimeters (Fig. 2.14).

A rough estimate shows that the ratio $|\omega_z/\omega_c|$ is typically very small, ranging from zero (straight running) up to about 0.01. It follows that usually $|(\omega_z/\omega_c)c_r|$ is negligible and points O and C have almost the same velocity.¹² However, particularly in competitions, it could be worthwhile to have a more detailed characterization of the behavior of the tire which takes into account even these minor aspects.

2.7.2 Zero Lateral Force

We can now discuss when the lateral force and the vertical moment are equal to zero.

According to (2.29), we have that $F_y = 0$ if

$$\tilde{F}_y \left(h, \gamma, \frac{V_{o_x}}{\omega_c}, \frac{V_{o_y}}{\omega_c}, \frac{\omega_z}{\omega_c} \right) = 0 \quad (2.39)$$

¹² However, in the *brush model*, and precisely on Sect. 11.1.5, the effect on C of the elastic compliance of the carcass is taken into account.

which means

$$\frac{V_{o_y}}{\omega_c} = f_y \left(h, \gamma, \frac{\omega_z}{\omega_c} \right) \quad (2.40)$$

where, as suggested by the experimental tests, there is no dependence on the value of V_{o_x} . Nevertheless, it seems that (2.40) does not have a simple structure like (2.33).

2.7.3 Zero Vertical Moment

Like in (2.30), the vertical moment with respect to O is zero, that is $M_z = 0$ if

$$\tilde{M}_z \left(h, \gamma, \frac{V_{o_x}}{\omega_c}, \frac{V_{o_y}}{\omega_c}, \frac{\omega_z}{\omega_c} \right) = 0 \quad (2.41)$$

which provides

$$\frac{V_{o_y}}{\omega_c} = f_z \left(h, \gamma, \frac{\omega_z}{\omega_c} \right) \quad (2.42)$$

where, like in (2.40), there is no dependence on the value of V_{o_x} . Also in this case, it is not possible to be more specific about the structure of this equation.

2.7.4 Zero Lateral Force and Zero Vertical Moment

However, the fulfilment of *both* conditions (2.40) and (2.42) together, that is $F_y = 0$ and $M_z = 0$, yields these results

$$V_{o_y}^r(h, \gamma) = V_{c_y}^r(h, \gamma) = 0 \quad (2.43)$$

$$\omega_z^r = -\omega_c \sin \gamma (1 - \varepsilon_r) \quad \Omega_z^r = \omega_c \sin \gamma \varepsilon_r(h, \gamma) \quad (2.44)$$

which have a simple structure. Sometimes $\varepsilon_r(h, \gamma)$ is called the *camber reduction factor* [20, p. 119], [21]. Usually, ε_r is almost constant for a given tire. Therefore, it does not really depend on h and γ

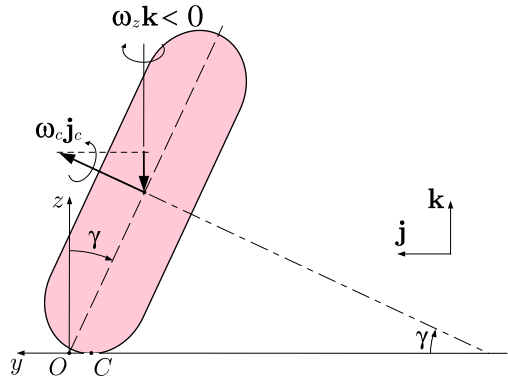
$$\varepsilon_r(h, \gamma) \simeq \varepsilon_r \quad (2.45)$$

A car tire has $0.4 < \varepsilon_r < 0.6$, while a motorcycle tire has ε_r almost equal to 0.

Equation (2.43) requires the lateral velocity of point O , and hence also of point C , to be equal to zero.

Equation (2.44) is equivalent to

Fig. 2.12 Yaw rate ω_z to compensate the camber induced spin ($\gamma > 0$, $\omega_z < 0$)



$$\frac{\omega_z^r}{\omega_c} = -\sin \gamma (1 - \varepsilon_r) \quad (2.46)$$

that is, the camber effects have to be compensated by the proper amount of yaw rate (Fig. 2.12). As a special case, to have pure rolling, the yaw rate ω_z must be equal to zero only when $\gamma = 0$.

The physical interpretation of (2.46) is that, to have $F_y = 0$ and $M_z = 0$, a cambered wheel with tire must go round as shown in Fig. 2.12 and in Fig. 2.16, with no lateral velocity and with a precise combination of ω_c and ω_z . Since no condition is set by (2.46) on the speed V_{c_x} , the radius of the circular path traced on the road by point C does not matter, unless we also want $F_x = 0$.

It is worth remarking that (2.43) alone does not imply zero lateral force (Fig. 2.13). A cambered wheel can yield a lateral force even if it has no lateral velocity. Similarly, (2.44) alone does not imply zero vertical moment.

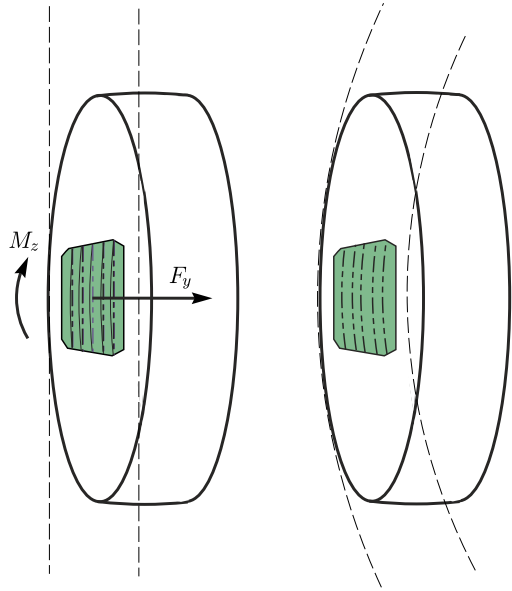
2.7.5 Pure Rolling Summary

Summing up, we have obtained the following kinematic conditions for a wheel with tire to be in what we have defined *pure rolling* in (2.25)–(2.27):

$$\begin{aligned} F_x = 0 & \iff V_{o_x}^r = \omega_c r_r(h, \gamma) + \omega_z c_r(h, \gamma) \\ \begin{cases} F_y = 0 \\ M_z = 0 \end{cases} & \iff \begin{cases} V_{o_y}^r = 0 \\ \omega_z^r = -\omega_c \sin \gamma (1 - \varepsilon_r) \end{cases} \end{aligned} \quad (2.47)$$

or, equivalently

Fig. 2.13 A cambered wheel under two different working conditions (see also Fig. 2.19)



$$\begin{aligned}
 F_x = 0 & \iff \frac{V_{c_x}^r}{\omega_c} = r_r(h, \gamma) \\
 \begin{cases} F_y = 0 \\ M_z = 0 \end{cases} & \iff \begin{cases} V_{c_y}^r = 0 \\ \frac{\omega_z^r}{\omega_c} = -\sin \gamma (1 - \varepsilon_r) \end{cases} \quad (2.48)
 \end{aligned}$$

These equations provide a sort of *reference condition* for the behavior of a wheel with tire (Fig. 2.14). Moreover, they are of key relevance for the subsequent definition of *tire slips*.

The complete characterization of pure rolling conditions essentially means obtaining the following functions (Fig. 2.14)

$$c_r(h, \gamma), \quad r_r(h, \gamma) \simeq r_r(\gamma), \quad \varepsilon_r(h, \gamma) \simeq \varepsilon_r \quad (2.49)$$

Of them, the rolling radius r_r is the most important, followed by the camber reduction factor ε_r . Of course, everything becomes much simpler if there is no camber: $c_r = 0$, and ε_r becomes irrelevant.

The fulfillment of only the first condition in (2.47) or (2.48) corresponds to longitudinal pure rolling. The fulfillment of only the last two conditions in (2.47) or (2.48) corresponds to lateral pure rolling.

It is worth recalling the main *assumptions* made (which are not always verified in real life):

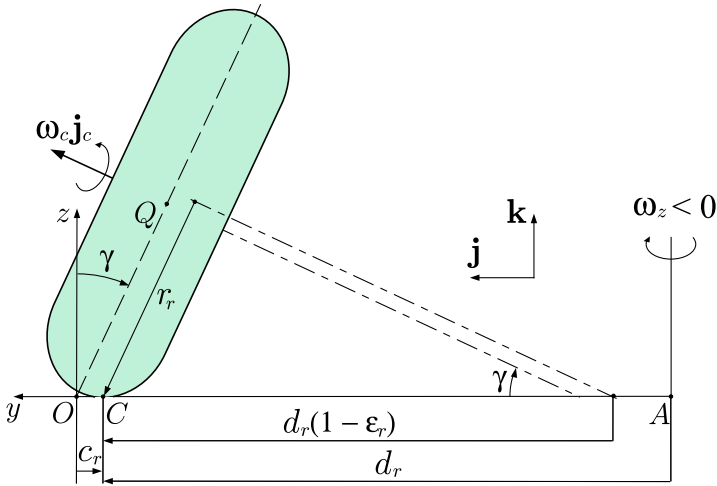


Fig. 2.14 Pure rolling of a cambered wheel with tire ($\gamma > 0$, $\omega_z < 0$, $c_r < 0$, $\epsilon_r > 0$)

- negligible inertial effects (five instead of six parameters);
- grip features unaffected by speed;
- point O defined as in Fig. 2.6;
- point C not affected by ω_z ;
- lateral velocity not affecting $F_x = 0$;
- longitudinal velocity not affecting $F_y = 0$ and $M_z = 0$.

2.7.6 Rolling Velocity and Rolling Yaw Rate

Point C and the first two equations in (2.48) provide the basis for the definition of the *rolling velocity* \mathbf{V}_r (Fig. 2.14)

$$\mathbf{V}_r = \omega_c r_r \mathbf{i} = V_r \mathbf{i} = V_{c_x}^r \mathbf{i} \tag{2.50}$$

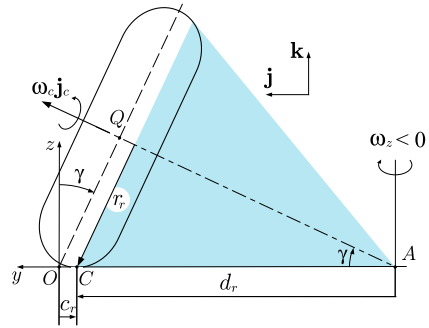
Similarly, the third equation in (2.47) leads to the definition of the *rolling yaw rate* ω_r of the reference system \mathbf{S}_w

$$\omega_r \mathbf{k} = -\omega_c \sin \gamma (1 - \epsilon_r) \mathbf{k} = \omega_z^r \mathbf{k} \tag{2.51}$$

Therefore, for a wheel with tire to be in total pure rolling it is necessary (according to (2.48)) that

$$\mathbf{V}_c = \mathbf{V}_r \quad \text{and} \quad \omega_z \mathbf{k} = \omega_r \mathbf{k} \tag{2.52}$$

Fig. 2.15 Pure rolling of a cambered rigid wheel ($\varepsilon_r = 0$)



To fulfill *both* these conditions we must move the wheel on a circular path centered at A , with radius $AC = d_r(h, \gamma) \mathbf{j}$ such that (Figs. 2.14 and 2.16)

$$\omega_z d_r = -\omega_c r_r \quad \text{with} \quad \omega_z = -\omega_c \sin \gamma (1 - \varepsilon_r) \quad (2.53)$$

which yields, for given γ , the radius d_r of the circular path for total pure rolling

$$d_r = \frac{r_r}{\sin \gamma (1 - \varepsilon_r)} \quad (2.54)$$

Typically the tire rolling radius r_r is slightly bigger than the distance of point C from the rim axis (Fig. 2.14). We recall that a car tire has $0.4 < \varepsilon_r < 0.6$, while a motorcycle tire has ε_r almost equal to 0. Therefore, if we take a car tire and a motorcycle tire with the same rolling radius r_r and the same camber angle γ , to have total pure rolling we must move the car tire on a circle about twice bigger than that of the motorcycle tire.

To help, hopefully, better understand Fig. 2.14, we also provide in Fig. 2.15 its counterpart in case of a rigid wheel. We can see that it behaves like a rolling rigid cone.

It is often stated that a free-rolling tire with a camber angle would move on a circular path [28, p. 163], [29, p. 128]. This statement is clearly incorrect. It should be reformulated as “a tire with camber must be moved on a definite circular path to have pure/free rolling” (Fig. 2.16). We are not doing dynamics here, but only investigating the (almost) steady-state behavior of wheels with tire. Therefore, we can say nothing about what a wheel would do by itself.

2.8 Definition of Tire Slips

Let us consider a wheel with tire under real operating conditions, that is *not* necessarily in pure rolling. The velocity of point C (defined in (2.35)) is called the *travel velocity* \mathbf{V}_c of the wheel (Fig. 2.14)

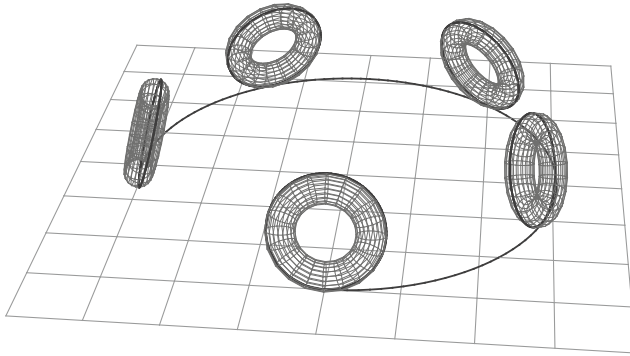


Fig. 2.16 Cambered wheel forced to move on a circular path (courtesy of M. Gabiccini)

$$\mathbf{V}_c = V_{c_x} \mathbf{i} + V_{c_y} \mathbf{j} = (V_{o_x} - \omega_z c_r) \mathbf{i} + V_{o_y} \mathbf{j} \quad (2.55)$$

The components of \mathbf{V}_c also have specific names: V_{c_x} is the *forward velocity* and V_{c_y} is the *lateral velocity*. In almost all practical cases, $\omega_z \simeq 0$, and hence

$$\mathbf{V}_o \simeq \mathbf{V}_c \quad (2.56)$$

To describe any steady-state conditions of a wheel with tire we need at least two parameters plus three kinematical quantities, as in (2.24). However, it is more informative to say how “distant” these three quantities are from pure rolling. It is therefore convenient to define the *slip velocity* [24] \mathbf{V}_s

$$\mathbf{V}_s = \mathbf{V}_c - \mathbf{V}_r \quad (2.57)$$

$$= (V_{c_x} \mathbf{i} + V_{c_y} \mathbf{j}) - \omega_c r_r \mathbf{i} \quad (2.58)$$

$$= [(V_{o_x} - \omega_z c_r) \mathbf{i} + V_{o_y} \mathbf{j}] - \omega_c r_r \mathbf{i} \quad (2.59)$$

$$= V_{s_x} \mathbf{i} + V_{s_y} \mathbf{j} \quad (2.60)$$

as the difference between the actual travel velocity (2.55) and the rolling velocity V_r .

Similarly, it is useful to define what can be called the *slip yaw rate* ω_{s_z}

$$\begin{aligned} \omega_{s_z} &= \omega_z - (-\omega_c \sin \gamma (1 - \varepsilon_r)) \\ &= \omega_z - \omega_r \end{aligned} \quad (2.61)$$

as the difference between the actual yaw rate ω_z of the reference system \mathbf{S}_w and the rolling yaw rate ω_r .

2.8.1 Theoretical Slips

Consistently with the assumed speed independence as in (2.24), it is meaningful to divide (2.57) and (2.61) by

$$V_r = \omega_c r_r \quad (2.62)$$

which leads to the definition of the well known (wheel with) tire slips σ_x , σ_y , and φ :

$$\sigma_x = \frac{V_{c_x} - \omega_c r_r}{\omega_c r_r} = \frac{V_{c_x} - V_r}{V_r} = \frac{V_{s_x}}{V_r} \quad (2.63)$$

$$\sigma_y = \frac{V_{c_y}}{\omega_c r_r} = \frac{V_{c_y}}{V_r} = \frac{V_{s_y}}{V_r} \quad (2.64)$$

$$\varphi = -\frac{\omega_z + \omega_c \sin \gamma (1 - \varepsilon_r)}{\omega_c r_r} = -\frac{\omega_z - \omega_r}{V_r} = -\frac{\omega_{s_z}}{V_r} \quad (2.65)$$

where the slip angle α was introduced in Fig. 2.6 and in (2.7). Car tires operate with very small camber angles. Therefore, we have $c_r \simeq 0$, that is $V_{o_x} \simeq V_{c_x}$ and $V_{o_y} \simeq V_{c_y}$.

These quantities have the following names [20, 21]:

σ_x theoretical longitudinal slip ($\sigma_x > 0$ means braking);

σ_y theoretical lateral slip ($\sigma_y > 0$ means a right turn);

φ spin slip.

The first two can be thought of as the components of the (*translational*) *theoretical slip* σ

$$\sigma = \sigma_x \mathbf{i} + \sigma_y \mathbf{j} = \frac{\mathbf{V}_c - \mathbf{V}_r}{V_r} = \frac{\mathbf{V}_s}{V_r} \quad (2.66)$$

while

$$\varphi = -\frac{\omega_z - \omega_r}{V_r} = -\frac{\omega_{s_z}}{V_r} \quad (2.67)$$

The longitudinal and lateral slips are dimensionless, whereas the spin slip is not: $[\varphi] = \text{m}^{-1}$.

Quite often tire tests are conducted with $\omega_z = 0$. In that case, $\mathbf{V}_o = \mathbf{V}_c$ and the spin slip simply becomes

$$\varphi = \frac{\omega_r}{V_r} = -\frac{\sin \gamma (1 - \varepsilon_r)}{r_r} \quad (2.68)$$

On the other hand, if only the yaw rate contribution is present (i.e., $\gamma = 0$), it is customary to speak of *turn slip* φ_t

$$\varphi_t = -\frac{\omega_z}{V_r} \quad (2.69)$$

Summing up, the *pure rolling* conditions (2.47) are therefore equivalent to

$$\begin{cases} \sigma_x = 0 \\ \sigma_y = 0 \\ \varphi = 0 \end{cases} \quad (2.70)$$

which look simpler, but are useless without the availability of r_r , c_r , and ε_r in (2.49).

2.8.2 The Simple Case (No Camber)

Since in most cars the camber angles are very small, the following simplified expressions can be safely used

$$\sigma_x = \frac{V_{o_x} - \omega_c r_r}{\omega_c r_r} = \frac{V_{o_x} - V_r}{V_r} \quad \text{and} \quad \sigma_y = \frac{V_{o_y}}{\omega_c r_r} = \frac{V_{o_y}}{V_r} \quad (2.71)$$

where the rolling radius r_r is almost constant. They are indeed much simpler than (2.63) and (2.64).

2.8.3 From Slips to Velocities

Inverting (2.63), (2.64), and (2.65), with the realistic assumption $c_r = 0$, we obtain

$$\begin{aligned} \frac{V_{o_x}}{\omega_c} &= (1 + \sigma_x)r_r \\ \frac{V_{o_y}}{\omega_c} &= \sigma_y r_r \\ \frac{\omega_z}{\omega_c} &= -\varphi r_r - \sin \gamma (1 - \varepsilon_r) \end{aligned} \quad (2.72)$$

2.8.4 (Not so) Practical Slips

Although, as will be shown, the theoretical slip σ is a better way to describe the tire behavior, it is common practice to use the components of the *practical slip* κ instead

$$\kappa_x = \left(\frac{V_r}{V_{c_x}} \right) \sigma_x = \frac{1}{1 + \sigma_x} \sigma_x = \frac{V_{c_x} - V_r}{V_{c_x}} \quad (2.73)$$

$$\kappa_y = \left(\frac{V_r}{V_{c_x}} \right) \sigma_y = \frac{1}{1 + \sigma_x} \sigma_y = \frac{V_{c_y}}{V_{c_x}} = -\tan \alpha \simeq -\alpha \quad (2.74)$$

or, conversely

$$\sigma_x = \frac{1}{1 - \kappa_x} \kappa_x = \kappa_x (1 + \kappa_x + O(\kappa_x^2)) \quad (2.75)$$

$$\sigma_y = \frac{1}{1 - \kappa_x} \kappa_y = \kappa_y (1 + \kappa_x + O(\kappa_x^2)) \quad (2.76)$$

which also shows that practical and theoretical slips are almost equal only when the longitudinal slip is small.

Practical slips are only apparently simpler and their use should be discouraged (for instance, have a look at Fig. 11.32 to appreciate why practical slips are not so practical). The *slip ratio* $\kappa = -\kappa_x$ is also often employed, along with the *slip angle* $\alpha \simeq -\kappa_y$. This approximation is quite good because the slip angle normally does not exceed 15° , that is 0.26 rad.

As discussed in [16, p. 39] and also in [20, p. 597], a number of slip ratio definitions are used worldwide [3, 6–8, 30]. A check, particularly of the sign conventions, is therefore advisable. This can be easily done for some typical conditions like locked wheel ($\omega_c = 0$), or spinning wheel ($\omega_c = \infty$). For instance, with the definitions given here we have $\sigma_x = +\infty$, $\kappa_x = 1$ and $\kappa = -1$ for a travelling locked wheel.

2.8.5 Tire Slips are Rim Slips Indeed

It is worth remarking that *all these tire slip quantities are just a way to describe the motion of the wheel rim, not of the tire*. Therefore they do not provide any direct information on the amount of sliding at any point of the contact patch.

More precisely, *sliding* or *adhesion* are *local* features of any point in the contact patch, whereas *slip* is a *global* property of the *rim* motion as a rigid body. They are completely different concepts. In this regard the name “tire slips” may be misleading. A more appropriate name would have been “rim slips”.

This statement is corroborated by the observation that all kinematic quantities introduced in this chapter refer to the rim motion. Actually, to find the kinematics of some points of the tire you have to await till the last chapter.

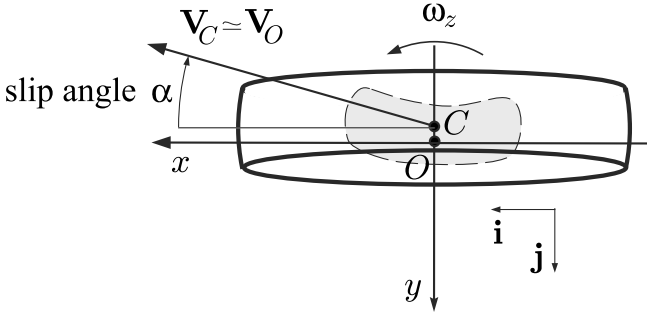


Fig. 2.17 Point O and point C , and slip angle α (top view)

2.8.6 Slip Angle

The *slip angle* α is defined as the angle between the rolling velocity $\mathbf{V}_r = V_r \mathbf{i}$ and the *travel velocity* $\mathbf{V}_c \simeq \mathbf{V}_o$ (Figs. 2.6 and 2.17)

$$\tan \alpha = -\frac{V_{c_y}}{V_{c_x}} \simeq -\frac{V_{o_y}}{V_{o_x}} \tag{2.77}$$

that is $V_{c_y} = -V_{c_x} \tan \alpha$, basically as in (2.7). For convenience, α is *positive* when measured *clockwise*, that is when it is like in Fig. 2.17.¹³

Of course, a non-sliding rigid wheel has a slip angle constantly equal to zero. On the other hand, a tire may very well exhibit slip angles. However, as will be shown, a wheel with tire can exchange with the road very high longitudinal and lateral forces still with *small* slip angles (as shown in Fig. 11.33). This is one of the reasons why a wheel with tire behaves quite close to a wheel, indeed.

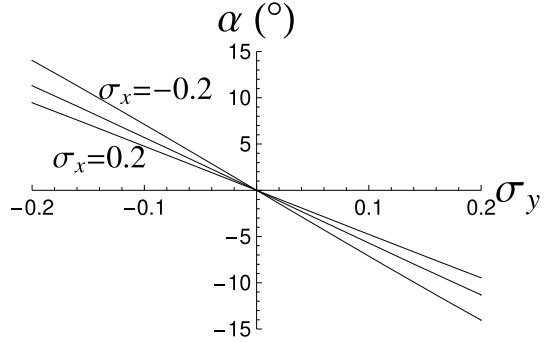
More precisely, (2.77) can be rewritten as

$$\tan \alpha = -\frac{\sigma_y}{1 + \sigma_x} = -\frac{\sigma_y}{\sigma_x} \left(\frac{\sigma}{\sigma + \frac{\sigma}{\sigma_x}} \right) \tag{2.78}$$

where $\sigma = |\boldsymbol{\sigma}| = \sqrt{\sigma_x^2 + \sigma_y^2}$. As shown in Fig. 2.18, if $\sigma < 0.2$ we have $|\alpha| < 10\text{deg}$. This is why real tires are built in such a way to provide the best performances with values of σ below 0.2, as will also be discussed later on with reference to Fig. 11.33.

¹³ All other angles are positive angles if measured counterclockwise, as usually done in mathematical writing.

Fig. 2.18 Slip angle α as a function of σ_x and σ_y



2.9 Grip Forces and Tire Slips

In (2.24) it was suggested that the steady-state global mechanical behavior of a wheel with tire could be described by means of forces and moments depending on (h, γ) to identify the rim position, and on other *three* kinematical parameters to determine the rim motion

$$\begin{aligned} F_x &= \tilde{F}_x \left(h, \gamma, \frac{V_{o_x}}{\omega_c}, \frac{V_{o_y}}{\omega_c}, \frac{\omega_z}{\omega_c} \right) \\ F_y &= \tilde{F}_y \left(h, \gamma, \frac{V_{o_x}}{\omega_c}, \frac{V_{o_y}}{\omega_c}, \frac{\omega_z}{\omega_c} \right) \\ M_z &= \tilde{M}_z \left(h, \gamma, \frac{V_{o_x}}{\omega_c}, \frac{V_{o_y}}{\omega_c}, \frac{\omega_z}{\omega_c} \right) \end{aligned} \quad (2.24')$$

Moreover, we have shown that the definition of the *pure rolling* conditions ($F_x = F_y = M_z = 0$) leads naturally to the definition of *three tire slips* σ_x , σ_y , and φ .

Inserting (2.72) into (2.24), we end up with these new functions

$$\begin{aligned} F_x &= \hat{F}_x(h, \gamma, \sigma_x, \sigma_y, \varphi) \\ F_y &= \hat{F}_y(h, \gamma, \sigma_x, \sigma_y, \varphi) \\ M_z &= \hat{M}_z(h, \gamma, \sigma_x, \sigma_y, \varphi) \end{aligned} \quad (2.79)$$

which provide a better and clearer description of the global mechanical behavior of a tire. Indeed, by definition

$$\begin{aligned} F_x &= \hat{F}_x(h, \gamma, 0, 0, 0) = 0 \\ F_y &= \hat{F}_y(h, \gamma, 0, 0, 0) = 0 \\ M_z &= \hat{M}_z(h, \gamma, 0, 0, 0) = 0 \end{aligned} \quad (2.80)$$

Instead of the vertical height h , it is customary to employ the vertical load F_z as an input variable. This can be safely done since

$$h = h(F_z, \gamma) \quad (2.81)$$

with very little influence by the other parameters (cf. (2.22)). Therefore, the (almost) steady-state global mechanical behavior of a wheel with tire moving not too fast on a flat road is conveniently described by the following functions

$$\begin{aligned} F_x &= F_x(F_z, \gamma, \sigma_x, \sigma_y, \varphi) \\ F_y &= F_y(F_z, \gamma, \sigma_x, \sigma_y, \varphi) \\ M_z &= M_z(F_z, \gamma, \sigma_x, \sigma_y, \varphi) \end{aligned} \quad (2.82)$$

Similarly, (2.49) can be recast as

$$c_r(F_z, \gamma) \simeq 0, \quad r_r(F_z, \gamma) \simeq r_r(\gamma), \quad \varepsilon_r(F_z, \gamma) \simeq \varepsilon_r \quad (2.83)$$

Unfortunately, it is common practice to employ the following functions, instead of (2.82)

$$\begin{aligned} F_x &= F_x^p(F_z, \gamma, \kappa_x, \alpha, \omega_z) \\ F_y &= F_y^p(F_z, \gamma, \kappa_x, \alpha, \omega_z) \\ M_z &= M_z^p(F_z, \gamma, \kappa_x, \alpha, \omega_z) \end{aligned} \quad (2.84)$$

They are, in principle, equivalent to (2.82). However, using the longitudinal practical slip κ_x , the slip angle α and the yaw rate ω_z provides a less systematic description of the tire mechanical behavior. It looks simpler, but ultimately it is not.

It is often overlooked that F_x , F_y and M_z (Eqs. (2.79) and (2.82)) depend on *both* the *camber angle* γ and the spin slip φ . In other words, two operating conditions with the same φ , but obtained with different γ 's, do not provide the same values of F_x , F_y and M_z , even if F_z , σ_x and σ_y are the same. For instance, the same value of φ can be obtained with no camber γ and positive yaw rate ω_z or with positive γ and no ω_z , as shown in Fig. 2.19. The two contact patches are certainly not equal to each other, and so the forces and moments. The same value of φ means that the rim has the same motion, but not the same position, if γ is different.

We remind that the moment M_z in (2.82) is with respect to a vertical axis passing through a point O chosen in quite an arbitrary way. Therefore, any attempt to attach a physical interpretation to M_z must take care of the position selected for O .

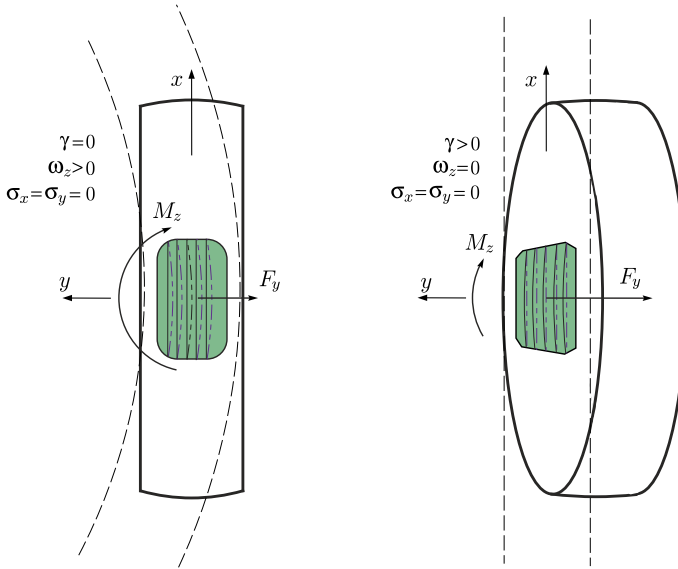


Fig. 2.19 Two different operating conditions, with the same spin slip $\varphi < 0$, but different camber angle γ (see also Fig. 2.13)

2.10 Tire Testing

Tire testing, as in Fig. 2.9, aims to fully identify the three functions (2.82) or (2.84), that is the *relationship* between the *motion* and *position* of the rim and the *force* and *moment* exchanged with the road through the contact patch

$$\text{rim kinematics} \quad \iff \quad \text{force and moment} \quad (2.85)$$

Actually, this goal had already been stated in Sect. 2.1. The difference is that now we have defined the *tire slips*, that is a precise set of parameters to control the *rim kinematics*.¹⁴

Indoor tire testing facilities (Fig. 2.9) usually have $\omega_z = 0$ in steady-state tests, and hence lack in generality by imposing a link between γ and φ , as shown in (2.68). However, in most practical applications in road vehicles we have $|\omega_z/\omega_c| < 0, 01$ and ω_z can indeed be neglected.¹⁵

Owing to (2.47) and (2.70), it is meaningful to perform experimental tests for the so-called *pure slip conditions*. Basically it means setting $\gamma = \varphi = 0$ and either $\sigma_y = 0$ or $\sigma_x = 0$. In the first case we have pure longitudinal slip and hence only the

¹⁴ Once again, we called *tire slips* what should be called *rim slips*.

¹⁵ In a step steer the steering wheel of a car may reach $\omega_z = 20^\circ/\text{s} = 0.35 \text{ rad/s}$. At a forward speed of 20 m/s, the same wheels have about $\omega_c = 80 \text{ rad/s}$. The contribution of ω_z to φ is therefore like a camber angle $\gamma \simeq 0, 5^\circ$.

longitudinal force $F_x = F_x(F_z, 0, \sigma_x, 0, 0)$, which is a very special case of (2.82). In the second case we have pure lateral slip, which allows for the experimental identification of the functions $F_y = F_y(F_z, 0, 0, \sigma_y, 0)$ and $M_z = M_z(F_z, 0, 0, \sigma_y, 0)$, which are also very special cases.

Unfortunately, the practical longitudinal slip κ_x and the slip angle α usually take the place of σ_x and σ_y , respectively [4].

2.10.1 Tests with Pure Longitudinal Slip

This kind of tests are often called drive/brake tests. Typically, they use longitudinal slip ratio sweeps with constant vertical load, constant forward velocity, and zero lateral velocity (i.e. zero slip angle).

Figure 2.20 shows the typical behavior of the longitudinal force F_x as a function of the practical longitudinal slip κ_x under pure braking conditions, for several values of the vertical load F_z . More precisely, it is the plot of $F_x^p(F_z, 0, \kappa_x, 0, 0)$. It is very important to note that:

- the maximum absolute value of F_x (i.e., the peak value F_x^{\max}) was obtained for $\kappa_x \simeq 0, 1$ (i.e., $\sigma_x \simeq 0, 11$);
- F_x grows *less than proportionally* with respect to the vertical load.

Both these aspects of tire behavior have great relevance in vehicle dynamics.

Also quite relevant are the values of the *longitudinal slip stiffness* C_{κ_x} , that is minus the slope of each curve at zero slip

$$C_{\kappa_x}(F_z) = - \left. \frac{\partial F_x^p}{\partial \kappa_x} \right|_{\kappa_x=0} \quad (2.86)$$

and the *global longitudinal friction coefficient* μ_p^x , that is the ratio between the peak value $F_x^{\max} = \max(|F_x^p|)$ and the corresponding vertical load

$$\mu_p^x(F_z) = \frac{F_x^{\max}}{F_z} \quad (2.87)$$

Typically, as shown in Fig. 2.21, it slightly decreases as the vertical load grows.

On the practical side, it is of some interest to observe that:

- the experimental values are affected by significant errors;
- the tests were carried out till $\kappa_x \simeq 0.3$, to avoid wheel locking and excessive damage to the tire tread;
- the offset of F_x for $\kappa_x = 0$ is due to the rolling resistance: the wheel was (erroneously, but typically) under free rolling conditions, not pure rolling.

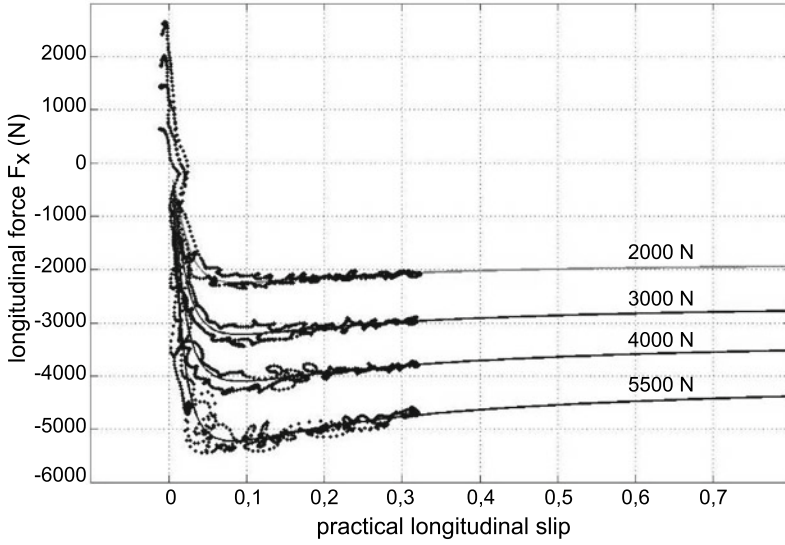
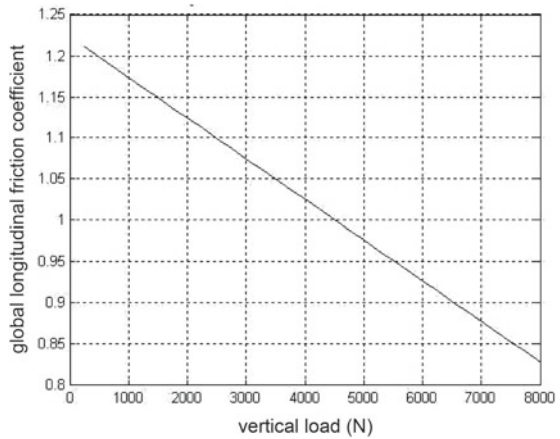


Fig. 2.20 Experimental results for a road tire: longitudinal force F_x vs practical longitudinal slip κ_x for four values of the vertical load F_z

Fig. 2.21 Global longitudinal friction coefficient μ_p^x vs vertical load F_z



2.10.2 Tests with Pure Lateral Slip

This kind of tests are also called cornering tests. Typically, they use slip angle sweeps with pure rolling, constant vertical load, and constant belt speed V_b (Fig. 2.9). It is worth noting that the wheel forward velocity is $V_{O_x} = V_b \cos \alpha$.

Figure 2.22 shows the typical behavior of the lateral force F_y as a function of the slip angle α , for three values of F_z . More precisely, it is the plot of $F_y^p(F_z, 0, 0, \alpha, 0)$. It is very important to note that:

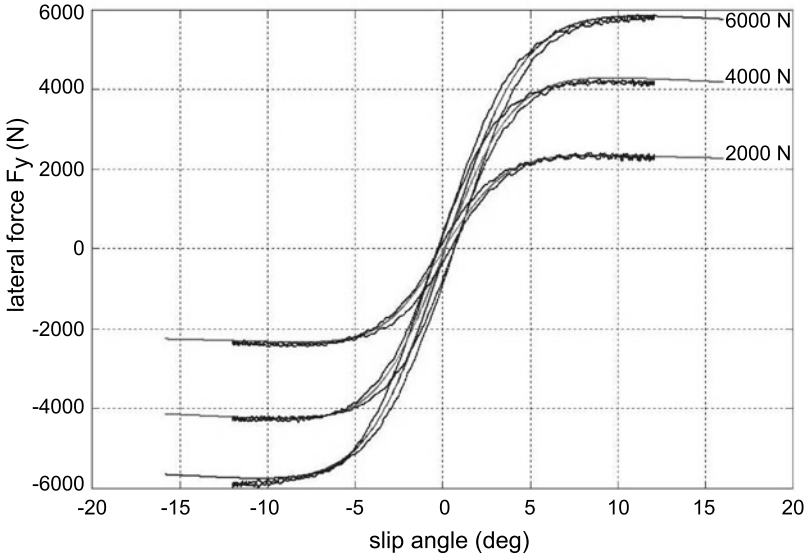


Fig. 2.22 Experimental results for a road tire: lateral force F_y vs slip angle α for three values of the vertical load F_z

- the maximum absolute value of F_y (i.e., the peak value F_y^{\max}) was obtained for $\alpha \simeq \pm 8^\circ$ (i.e., $\tan \alpha = -\sigma_y = \pm 0,14$);
- F_y grows *less than proportionally* with respect to the vertical load.

Also quite relevant are the values of the *lateral slip stiffness* C_α , also called *cornering stiffness*

$$C_\alpha(F_z) = \left. \frac{\partial F_y^p}{\partial \alpha} \right|_{\alpha=0} \tag{2.88}$$

that is the slope at the origin. As shown in Fig. 2.23, C_α grows less than proportionally with F_z , and actually it can even decrease at exceedingly high values of the vertical load.

Another important quantity is the *global lateral friction coefficient* μ_p^y , that is the ratio between the peak value $F_y^{\max} = \max(|F_y^p|)$ and the vertical load

$$\mu_p^y(F_z) = \frac{F_y^{\max}}{F_z} \tag{2.89}$$

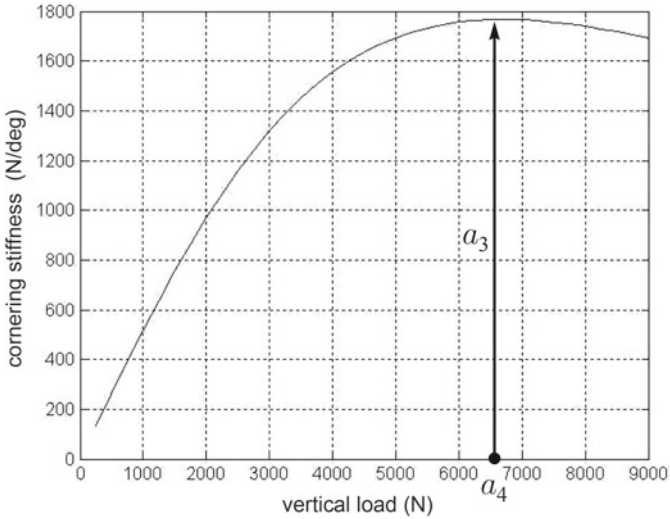


Fig. 2.23 Cornering stiffness C_α vs vertical load F_z

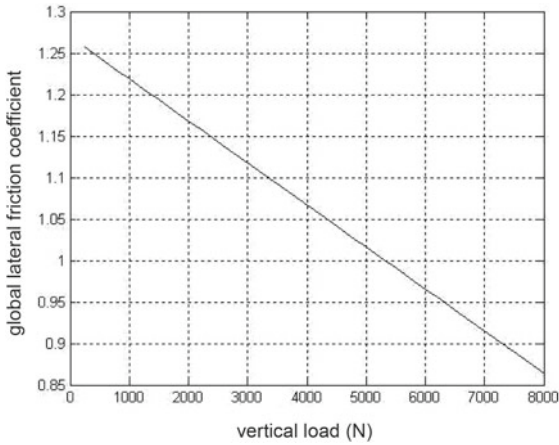


Fig. 2.24 Global lateral friction coefficient μ_p^y vs vertical load F_z

As shown in Fig. 2.24, it slightly decreases with F_z .

Comparing Figs. 2.21 and 2.24 we see that similar peak values for F_x and F_y are obtained for the same vertical load, that is $\mu_p^x \simeq \mu_p^y$. Typically, μ_p^x is slightly greater than μ_p^y .

On the practical side it is to note that:

- the experimental values are affected by small errors;
- the tests were carried out till $\alpha \simeq 12^\circ$, to avoid damaging the tire tread.

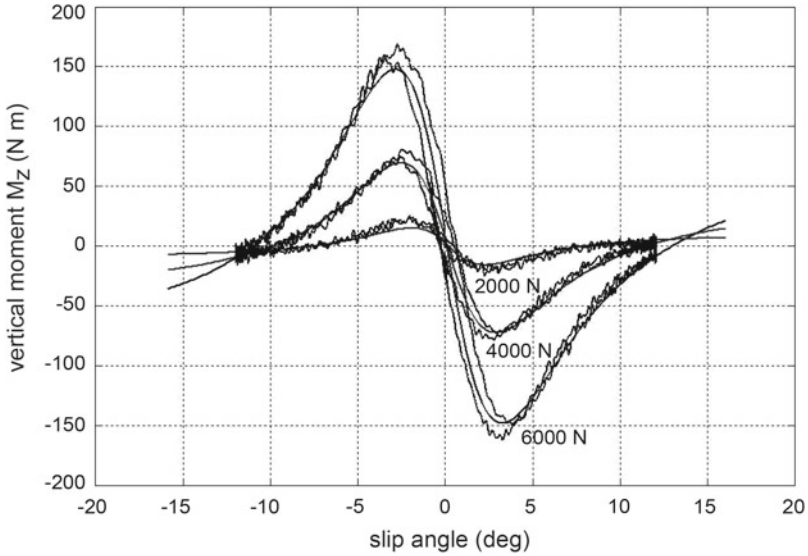


Fig. 2.25 Experimental results: vertical moment M_z vs slip angle α for three values of the vertical load F_z

Figure 2.25 shows an example of the vertical moment M_z as a function of the slip angle α , for three values of F_z , that is the plot of $M_z^P(F_z, 0, 0, \alpha, 0)$. The tests are the same of Fig. 2.22 and similar observations apply.

The behavior of $M_z(\alpha)$ is obviously very much affected by the position of the z -axis, which should be always clearly stated. Therefore, it is hard to speak of “typical behavior” of M_z , unless there is general agreement on where to locate the origin O of the reference system. This aspect could be quite relevant in the comparison and interpretation of tests performed by different institutions, particularly for motorcycle tires at large camber angles.

2.11 Magic Formula

In vehicle dynamics it is useful to have mathematical functions that fit experimental tire response curves, like those in Figs. 2.20 and 2.22. Usually, these curves have similar shapes: they grow less than proportionally, reach a maximum and then tend to a horizontal asymptote. Among the very many functions that share all these features, there is one which is almost exclusively used in vehicle dynamics. It was called *Magic Formula* (MF) by its inventors [1, 2, 23].

Although, over the years, several versions of the Magic Formula have been developed, they are all based on the following anti-symmetric function [20, 24]

$$y(x) = D \sin\{C \arctan[Bx - E(Bx - \arctan(Bx))]\} \quad (2.90)$$

where the four coefficients are usually referred to as

$$\begin{aligned} B & \text{ stiffness factor} \\ C & \text{ shape factor} \\ D & \text{ peak value} \\ E & \text{ curvature factor} \end{aligned} \quad (2.91)$$

Of course, y can be either F_x or F_y , with x being the corresponding practical or theoretical slip component.

The Magic Formula belongs to the so-called *empirical tire models*, in the sense that they mimic some experimental curves, like those in Figs. 2.20 and 2.22, without any modeling of the physical phenomena involved in tire mechanics.

2.11.1 Magic Formula Properties

Let

$$B > 0 \quad E < 1 \quad \text{and} \quad 1 < C < 2 \quad (2.92)$$

It is quite easy to show that the Magic Formula has the following properties:

- $y(0) = 0$;
- $y'(0) = BCD$ (slope at the origin);
- $y''(0) = 0$;
- $y'''(0) < 0$, if $-(1 + C^2/2) < E$;
- the function is limited: $|y(x)| \leq D$;
- the function has a relative maximum $y_m = y(x_m) = D$, with x_m such that

$$B(1 - E)x_m + E \arctan(Bx_m) = \tan(\pi/(2C)); \quad (2.93)$$

- the value of the horizontal asymptote is

$$y_a = \lim_{x \rightarrow +\infty} y(x) = D \sin(C\pi/2) \quad (2.94)$$

2.11.2 Fitting of Experimental Data

Probably, the most relevant features of an experimental curve like in Fig. 2.22 are the peak value y_m with the corresponding abscissa x_m , the asymptotic value y_a and the slope at the origin $y'(0)$. Therefore, to determine the four coefficients a possible procedure is as follows. First set the peak value

$$D = y_m \tag{2.95}$$

then compute the shape factor C employing (2.94)¹⁶

$$C = 2 - \frac{2}{\pi} \arcsin\left(\frac{y_a}{D}\right) \tag{2.96}$$

obtain the stiffness factor B as

$$B = \frac{y'(0)}{CD} \tag{2.97}$$

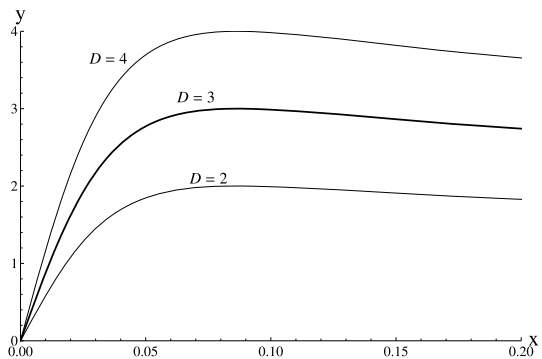
and, finally, determine the curvature factor E from (2.93), that is by fitting the value of x_m

$$E = \frac{Bx_m - \tan(\pi/(2C))}{Bx_m - \arctan(Bx_m)} \tag{2.98}$$

It is important that $y_a < y_m$. If they are equal (or almost equal), an unexpected plot may result.

How the four coefficients affect the Magic Formula plot is shown in Figs. 2.26, 2.27, 2.28 and 2.29. In all these plots, the thick line was obtained with $D = 3$, $C = 1.5$, $B = 20$ and $E = 0$.

Fig. 2.26 Changing the peak value D in the Magic Formula



¹⁶ $\sin(C\pi/2) = \sin((2 - C)\pi/2)$, since $1 < C < 2$.

Fig. 2.27 Changing the shape factor C in the Magic Formula

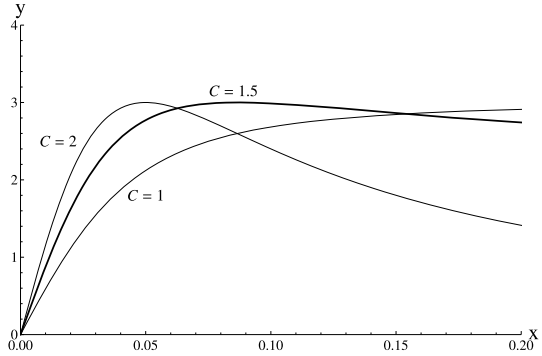


Fig. 2.28 Changing the stiffness factor B in the Magic Formula

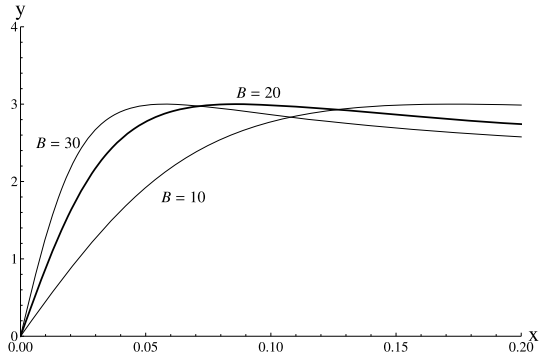
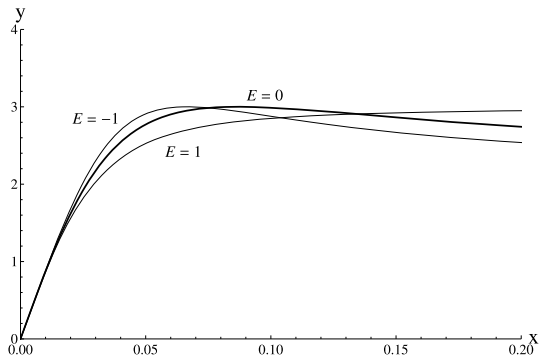


Fig. 2.29 Changing the curvature factor E in the Magic Formula



The Magic Formula usually does a good job at approximating experimental curves like in Fig. 2.20 and Fig. 2.22, although, with only four coefficients, the fitting may not be of uniform quality at all points. This aspect will be addressed in Figs. 11.25 and 11.26.

2.11.3 Vertical Load Dependence

Quite often, some coefficients of the Magic Formula are made dependent on the vertical load F_z . According to Figs. 2.21 and 2.24, the global friction coefficient $\mu_p = D/F_z$ decreases almost linearly with F_z , and hence it is quite reasonable to assume

$$D = D(F_z) = \mu_p F_z = (a_1 F_z + a_2) F_z \quad (2.99)$$

with $a_1 < 0$.

To mimic the pattern shown in Fig. 2.23 for the slope at the origin $y'(0)$, the following formula has been suggested [24]

$$BCD = y'(0) = a_3 \sin(2 \arctan(F_z/a_4)) \quad (2.100)$$

Actually, the formula to be used is

$$B = B(F_z) = \frac{y'(0)}{CD(F_z)} = \frac{a_3 \sin(2 \arctan(F_z/a_4))}{C (a_1 F_z + a_2) F_z} \quad (2.101)$$

According to Figs. 2.23 and 2.24, typical values for a road car tire may be $a_1 = -0.05 \text{ kN}^{-1}$, $a_2 = 1.25$, $a_3 = 32 \text{ kN/rad} = 1.8 \text{ kN/deg}$, $a_4 = 6.5 \text{ kN}$. The interpretation of the parameters a_3 and a_4 is shown in Fig. 2.23.

2.11.4 Horizontal and Vertical Shifts

A simple generalization of the MF is by adding a vertical shift y_v and/or a horizontal shift x_h

$$y(x) = y_v + D \sin \left\{ C \arctan \left[B(x + x_h) - E \left(B(x + x_h) - \arctan(B(x + x_h)) \right) \right] \right\} \quad (2.102)$$

This version of the MF can cope with rolling resistance and/or tire conicity etc.

2.11.5 Camber Dependence

The camber angle γ has a small, but significant, effect on the lateral force F_y , as will be shown in Figs. 2.37 and 2.38. Therefore, the coefficients of the MF (2.102) should depend on the camber angle as well. In particular, the Pacejka '94 coefficients are

$$\begin{aligned}
C &= a_0 \\
D &= (a_1 F_z + a_2) F_z (1 - a_{15} \gamma^2) \\
BCD &= a_3 \sin(2 \arctan(F_z/a_4))(1 - a_5 |\gamma|) \\
B &= BCD/(CD) \\
E &= (a_6 F_z + a_7)(1 - (a_{16} \gamma + a_{17}) \operatorname{sign}(x + x_h)) \\
x_h &= a_8 F_z + a_9 + a_{10} \gamma \\
y_v &= a_{11} F_z + a_{12} + (a_{13} F_z + a_{14}) \gamma F_z
\end{aligned} \tag{2.103}$$

Fitting 18 coefficients may not be an easy task.

An extensive description of the Magic Formula and all its subtleties can be found in [20]. Additional information is available in [11].

2.12 Mechanics of the Wheel with Tire

The main result of this chapter is that to describe the steady-state mechanics of the wheel with tire we need, as a minimum, the functions given in (2.82), that is

$$\begin{aligned}
F_x &= F_x(F_z, \gamma, \sigma_x, \sigma_y, \varphi) \\
F_y &= F_y(F_z, \gamma, \sigma_x, \sigma_y, \varphi) \\
M_z &= M_z(F_z, \gamma, \sigma_x, \sigma_y, \varphi)
\end{aligned} \tag{2.82'}$$

However, taking (2.68) into account, an even simpler formulation for the tire constitutive equations can be adopted in most cases

$$\begin{aligned}
F_x &= F_x(F_z, \gamma, \sigma_x, \sigma_y) \\
F_y &= F_y(F_z, \gamma, \sigma_x, \sigma_y) \\
M_z &= M_z(F_z, \gamma, \sigma_x, \sigma_y)
\end{aligned} \tag{2.104}$$

Of course, they are not the whole story, and the interested reader will find in Chap. 11 many hints to better understand steady-state and also transient tire behavior.

But let us go back to (2.104). It is very informative to analyze the functions in (2.104) varying only one parameter at the time, while keeping constant (often equal to zero) all the others. These plots are like the filtered (smoothed) version of the experimental plots presented in Sect. 2.10 on tire tests. They are something that any vehicle engineer should always have clear in mind.

The plots hereafter were drawn employing the Magic Formula with the parameters reported below Eq. (2.101). The shape factor C was set equal to 1.65 for the plots of F_x , and equal to 1.3 for the plots of F_y . All forces are in kN.

2.12.1 Braking/Driving

We start with the function $F_x(F_z, 0, \sigma_x, 0) = F_x(\sigma_x)$. Most tires under pure longitudinal slip σ_x behave like in Fig. 2.30. Very near the origin the function is almost linear, but soon becomes strongly nonlinear. Relative maximum/minimum points are attained for $|\sigma_x| \simeq 0.1$. Positive σ_x means braking, negative σ_x means driving.

The effect of changing the vertical load F_z is also shown in Fig. 2.30. Obviously, the higher F_z , the higher $F_x(\sigma_x)$. However, as already mentioned on Sect. 2.10.1 and shown in Fig. 2.20, the growth of F_x with respect to F_z is less than proportional, particularly for low values of $|\sigma_x|$. This is more clearly shown in Fig. 2.31, where we see that the vertical order of the plots of the normalized longitudinal force $F_x^n = F_x(\sigma_x)/F_z$ is reversed with respect to Fig. 2.30. This kind of drawings are often called μ -slip curves.

Fig. 2.30 Longitudinal force F_x due to pure longitudinal slip σ_x , for decreasing vertical loads F_z . More precisely $F_x = F_x(F_z, 0, \sigma_x, 0)$

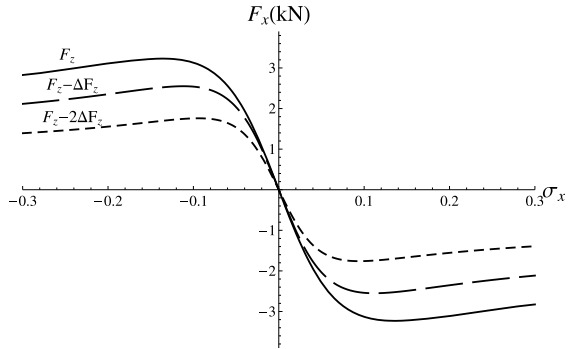
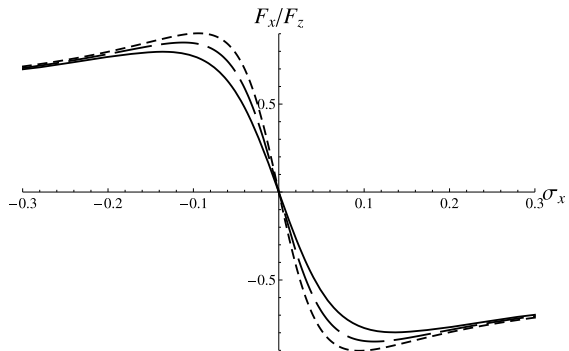


Fig. 2.31 Normalized longitudinal force F_x/F_z due to pure longitudinal slip σ_x , for decreasing vertical loads F_z (line dashing as in Fig. 2.30)



2.12.2 Cornering

Now we consider the function $F_y(F_z, 0, 0, \sigma_y) = F_y(\sigma_y)$. Most tires under pure lateral slip σ_y behave like in Fig. 2.32. Very near the origin the function is almost linear, but it soon becomes strongly nonlinear. Relative maximum/minimum points are attained for $|\sigma_y| \simeq 0.1$. Positive σ_y means negative slip angle α , and viceversa.

Moreover, the effect of changing the vertical load F_z is shown in Fig. 2.32. Again, the growth of F_y with respect to F_z is less than proportional, particularly for low values of $|\sigma_y|$. It is precisely this nonlinearity that is, let us say, activated by anti-roll bars to modify the handling setup of a car. This phenomenon is shown in Fig. 2.33, where we see that the vertical order of the plots of the normalized lateral force $F_y^n = F_y(\sigma_y)/F_z$ is reversed with respect to Fig. 2.32.

It should be noted that functions $F_x(F_z, 0, \sigma_x, 0)$ and $F_y(F_z, 0, 0, \sigma_y)$ behave in a similar way.

The experimental counterpart of Fig. 2.32 was presented in Fig. 2.22.

Fig. 2.32 Lateral force F_y due to pure lateral slip σ_y , for decreasing vertical loads F_z . More precisely $F_y = F_y(F_z, 0, 0, \sigma_y)$

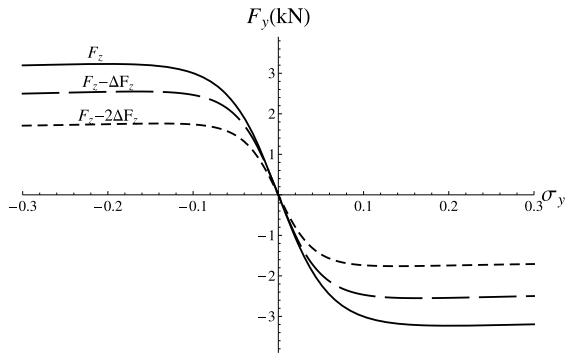
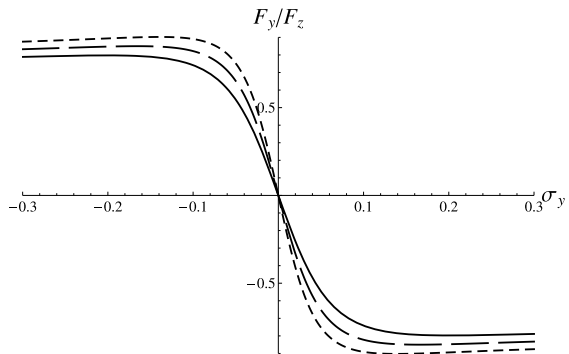


Fig. 2.33 Normalized lateral force F_y/F_z due to pure lateral slip σ_y , for decreasing vertical loads F_z (line dashing as in Fig. 2.32)



2.12.3 Combined

The simultaneous application of σ_x and σ_y affects the grip forces F_x and F_y as shown in Figs. 2.34 and 2.35. Basically, the total force \mathbf{F} , with components F_x and F_y , is directed like the slip vector $\boldsymbol{\sigma}$, with opposite sign, and has a magnitude almost dependent on $\sigma = |\boldsymbol{\sigma}|$

$$\begin{aligned} F_x &= -\frac{\sigma_x}{\sigma} F_t(\sigma), \\ F_y &= -\frac{\sigma_y}{\sigma} F_t(\sigma) \end{aligned} \tag{2.105}$$

The function $F_t(\sigma)$ can be represented by the Magic Formula.

The tire behavior under combined operating conditions will be thoroughly addressed in Chap 11, where the tire brush model will be developed. At the moment you may have a look at Fig. 11.28, and also at Fig. 11.29.

It is worth noting that the two Figs. 2.34 and 2.35 convey, in different ways, exactly the same information.

Another useful plot is the one shown in Fig. 2.36. For any combination of (σ_x, σ_y) , a point in the plane (F_x, F_y) is obtained. All these points fall within a circle of radius F_t^{\max} , usually called the *friction circle*. Lines with constant σ_y are also drawn in Fig. 2.36. Lines with constant σ_x are similar, but rotated by 90 degrees around the origin, as shown in Fig. 11.38b.

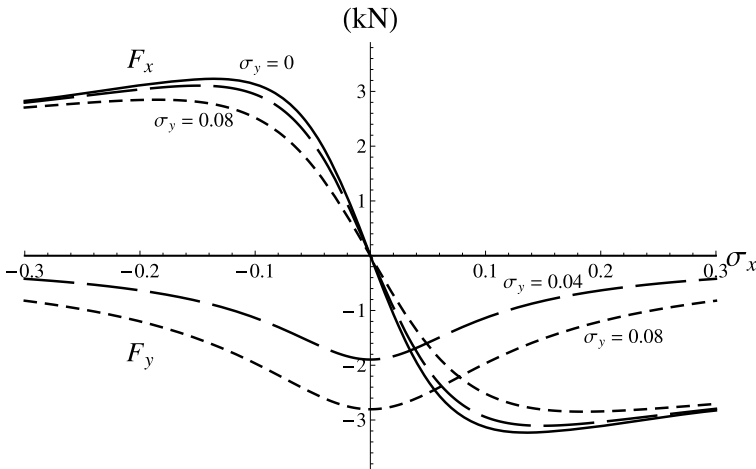


Fig. 2.34 Longitudinal force F_x and lateral force F_y due to combined longitudinal slip σ_x and lateral slip σ_y , for constant vertical load F_z . More precisely $F_x = F_x(F_z, 0, \sigma_x, \sigma_y)$ and $F_y = F_y(F_z, 0, \sigma_x, \sigma_y)$

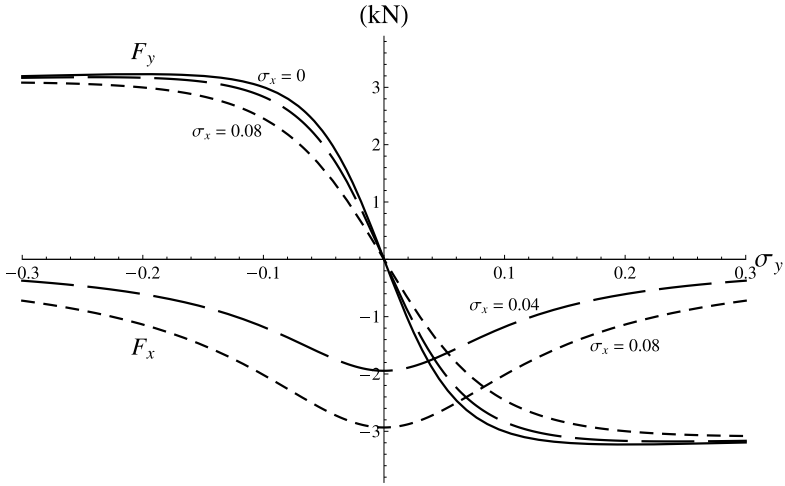


Fig. 2.35 Longitudinal force F_x and lateral force F_y due to combined longitudinal slip σ_x and lateral slip σ_y , for constant vertical load F_z . More precisely $F_x = F_x(F_z, 0, \sigma_x, \sigma_y)$ and $F_y = F_y(F_z, 0, \sigma_x, \sigma_y)$

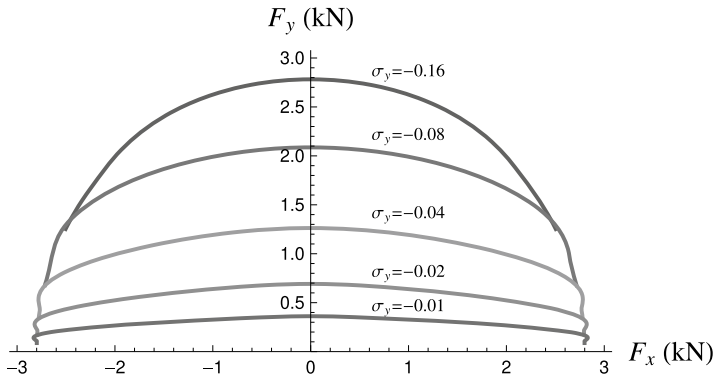


Fig. 2.36 Friction circle with lines at constant σ_y

2.12.4 Camber

Also quite relevant is the effect of the camber angle γ , alone or in combination with σ_y , on the lateral force F_y , as shown in Fig. 2.37 and, for better clarity, also in Fig. 2.38. We see that the camber effects are much stronger at low values of σ_y . However, a right amount of camber can increase a little the maximum lateral force, thus improving the car handling performance.

Fig. 2.37 Lateral force F_y due to lateral slip σ_y , for different values of the camber angle γ and constant vertical load F_z . More precisely $F_y = F_y(F_z, \gamma, 0, \sigma_y)$

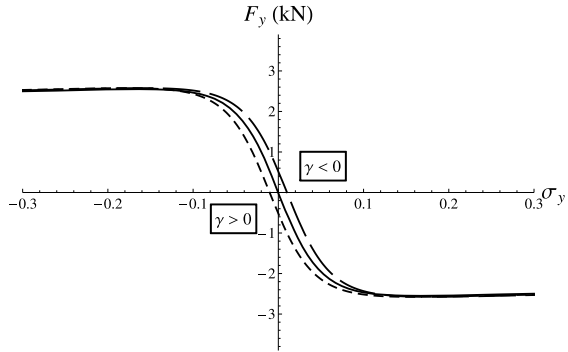
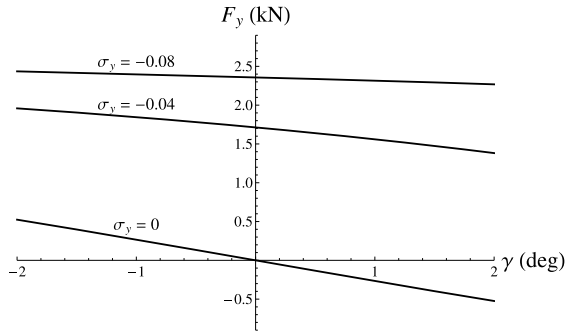


Fig. 2.38 Lateral force F_y due to camber angle γ , for different values of the lateral slip σ_y and constant vertical load F_z . More precisely $F_y = F_y(F_z, \gamma, 0, \sigma_y)$



2.12.5 Grip

Finally, the effect of decreasing the grip coefficient μ is investigated. We see in Figs. 2.39 and 2.40 that, as expected, we get lower maximum tangential forces. However, it should also be noted that changing the grip does not affect the slope of the curves at the origin. The reason is that near the origin the tangential force is, by definition, very small, and hence the tire behavior is mainly affected by the tire structure, not by the available amount of grip.

2.12.6 Vertical Moment

The vertical moment M_z as a function of σ_y , with $\sigma_x = 0$, behaves as shown in Fig. 2.41. The reasons for this behavior will be discussed in Chap. 11. Basically, since $M_z = F_t d_t$ (Fig. 2.7), it is the product of a growing force times a decreasing length. It is zero when either of the two is zero.

For much more information on the mechanics of the wheel with tire we suggest to carefully read Chap. 11 on tire models.

Fig. 2.39 Longitudinal force F_x due to pure longitudinal slip σ_x , for constant vertical load F_z and decreasing grip

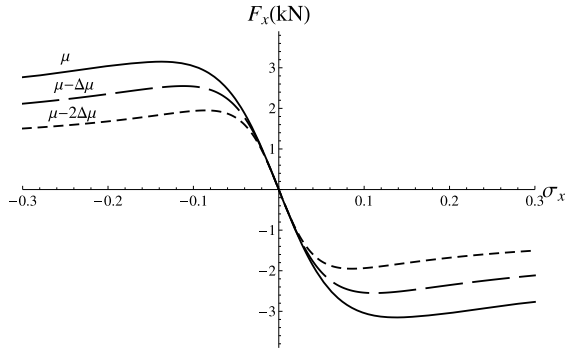


Fig. 2.40 Lateral force F_y due to pure lateral slip σ_y , for constant vertical load F_z and decreasing grip

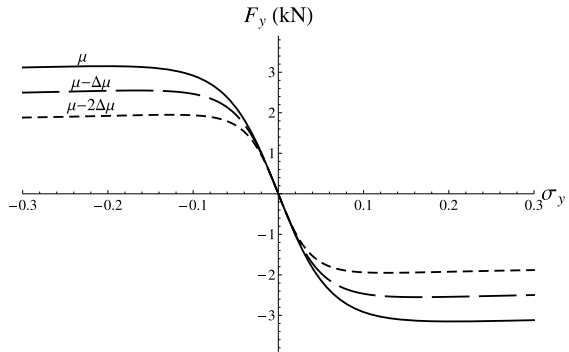
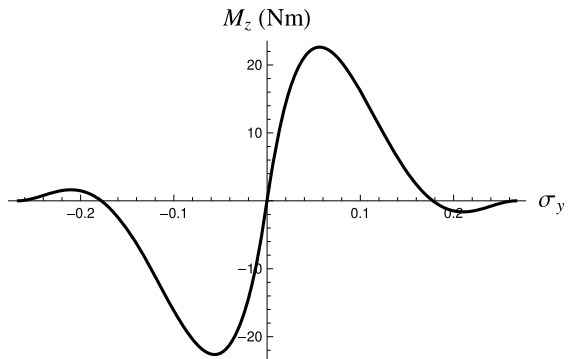


Fig. 2.41 Vertical moment M_z due to pure lateral slip σ_y



2.13 Rolling Resistance

When a car is driven in a straight line without braking or accelerating, the rolling resistance is mainly caused by the *hysteresis* in the tire due to the deflection of the carcass while rolling. Microslippage in the footprint accounts for less than 5% of total rolling resistance. As shown schematically in Figs. 2.42 and 2.43, the normal pressure p in the leading half of the contact patch is higher than that in the trailing

Fig. 2.42 Torque rolling:
 $T = F_z e_x$ and $F_x = 0$

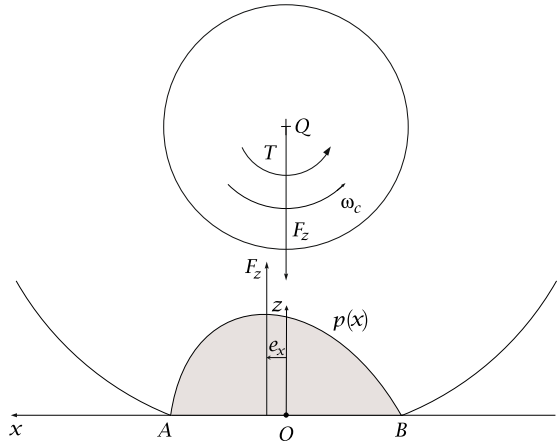
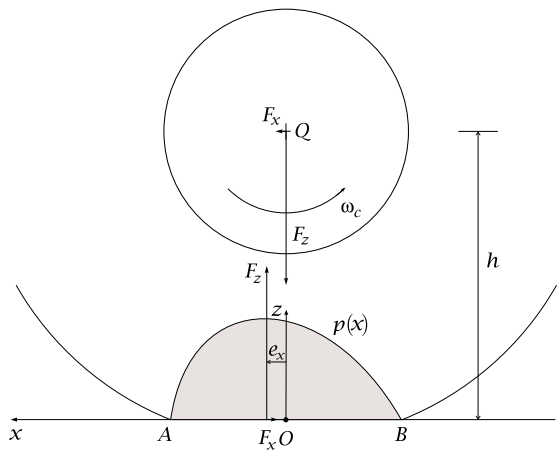


Fig. 2.43 Tractive rolling:
 $F_x h = F_z e_x$ and $T = 0$



half. Therefore, the vertical resultant $F_z \mathbf{k}$ of the pressure distribution is offset by e_x towards the front of the contact patch, thus generating a *rolling resistance moment*

$$M_y = -F_z e_x \tag{2.106}$$

as already done in (2.10).

The main source of energy dissipation is therefore the visco-elasticity of the materials of which tires are made. Visco-elastic materials lose energy in the form of heat whenever they are deformed. Deformation-induced energy dissipation is the cause of about 90% of rolling resistance [15, 30].

A number of tire operating conditions affect rolling resistance. The most important are load, inflation pressure and temperature. However, as speed increases, tire's

internal temperature rises, offsetting some of the increased hysteresis. Therefore, the tire rolling resistance moment is almost constant on a relatively wide range of speeds.

There are basically two different ways to balance the *rolling resistance moment*

$$M_y = -F_z e_x \quad (2.107)$$

- torque rolling: $T = F_z e_x$ and $F_x = 0$ (Fig. 2.42);
- tractive rolling: $F_x = F_z e_x / h = F_z f_r$ and $T = 0$ (Fig. 2.43).

In the first case (torque rolling) we apply a little torque $T \mathbf{j}$ to the rim to balance the moment $M_y \mathbf{j}$, while keeping $F_x = 0$. In the second case (tractive rolling), we apply a horizontal force $F_x \mathbf{i}$ to the center of the rim, which requires an opposite force to be generated in the contact patch.

In case of tractive rolling, we can define the *rolling resistance coefficient* f_r

$$f_r = \frac{e_x}{h} = \frac{F_x}{F_z} \quad (2.108)$$

The values given by tire manufacturers are measured on test drums, usually at 80 km/h in accordance with ISO measurement standards. A typical value of the rolling resistance coefficient f_r for a road car tire is $f_r = 0.006\text{--}0.016$.

2.14 Driving Torque and Tractive Force

Let us apply a (large) driving torque $\mathbf{T} = T \mathbf{j}_c$ to the rim, thus generating a tractive force F_x . Neglecting the (small) moment of inertia of the rim, we have

$$\begin{aligned} \mathbf{T} = T \mathbf{j}_c &= -((\mathbf{QO} \times \mathbf{F} + \mathbf{M}_O) \cdot \mathbf{j}_c) \mathbf{j}_c \\ &= \left(F_x \frac{h}{\cos \gamma} - M_y \cos \gamma - M_z \sin \gamma \right) \mathbf{j}_c \end{aligned} \quad (2.109)$$

where (2.2) and (2.5) were employed. This expression is fairly simple because the rim axis y_c intersects the z -axis and is perpendicular to the x -axis (Figs. 2.6 and 2.7).

A driving torque $T > 0$ applied to the rim can have a large impact on the offset e_x (Fig. 2.44), and hence on the rolling resistance. As the magnitude of torque applied increases, the rolling resistance first increases mildly. Then, when slippage at the road surface becomes significant, the rolling resistance increases very rapidly. This rapid increase occurs as the maximum torque that the tire can transmit is approached [5, p. 496].

Fig. 2.44 Applying a really large driving torque



2.14.1 Tractive Force

It is often of interest to evaluate the tractive force F_x generated by a drive torque T . As shown in Fig. 2.45, if $\gamma = 0$, Eq. (2.109) becomes

$$T = F_x h + F_z e_x = F_x (h + e_z) = F_x a \tag{2.110}$$

where, obviously

$$e_z = F_z \frac{e_x}{F_x} \tag{2.111}$$

We see that, ultimately, to know F_x we have to estimate the *drive lever arm* a .

In [32, p. 51] it is shown that this lever arm a can be approximated by the rolling radius r_r

$$a \simeq r_r \tag{2.112}$$

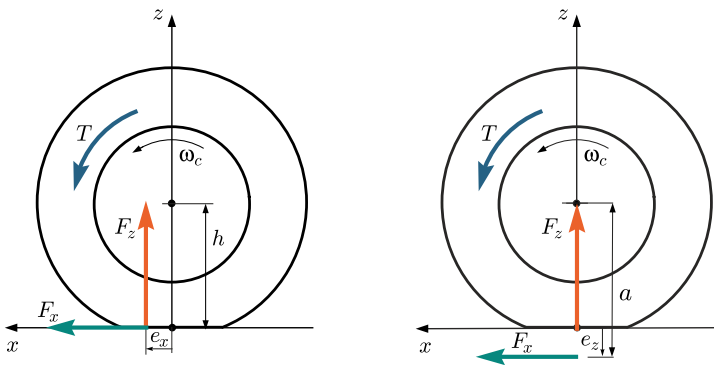


Fig. 2.45 Driving torque T and tractive force F_x : two fully equivalent schemes

Indeed, from power balance and (2.50) we have that

$$T\omega_c = F_x V_r = F_x \omega_c r_r \quad (2.113)$$

It is worth noting that the center of the wheel (and hence the vehicle) moves with speed $V_x = (1 + \sigma_x)\omega_c r_r$, with $\sigma_x < 0$.

From (2.38) and (2.110)–(2.112) we obtain that the ratio e_x/F_x should be almost constant, for given F_z .

2.15 Exercises

2.15.1 Pure Rolling

Explain the difference between torque rolling and trailing rolling in a tire.

Solution

See Sect. 2.13.

2.15.2 Theoretical and Practical Slips

Obtain the relationships between theoretical and practical slip components.

Solution

See (2.73) and (2.74).

2.15.3 Tire Translational Slips and Slip Angle

Find the tire slip angle α in the following cases:

1. $\sigma_y = 0$;
2. $\sigma_y = 0.1$ and $\sigma_x = 0$ (only cornering);
3. $\sigma_y = 0.1$ and $\sigma_x = 0.1$ (cornering and braking);
4. $\sigma_y = 0.1$ and $\sigma_x = -0.1$ (cornering and driving).

Solution

To solve these problems we can use (2.78).

The first case is trivial. Obviously $\alpha = 0$.

The second case is also quite simple, since $\sigma_x = 0$. Therefore, $\alpha = -\arctan(0.1) = -5.7^\circ$.

In the third case we have both lateral and longitudinal slip (cornering and braking). Still according to (2.78), $\alpha = -\arctan(0.1/(1 + 0.1)) = -5.2^\circ$.

Case number four is similar to case number three, but with negative σ_x (cornering and driving). It provides $\alpha = -\arctan(0.1/(1 - 0.1)) = -6.3^\circ$.

It is quite interesting to observe how the longitudinal slip affects the slip angle, for given lateral slip. All these results apply to all tires, regardless of their size, type, etc., and are not affected by camber and spin slip. We have simply done kinematics of the rigid rim.

2.15.4 Tire Spin Slip and Camber Angle

Let a tire have a rolling radius $r_r = 0.262$ m and a camber reduction factor $\varepsilon_r = 0.5$. We set the camber angle $\gamma = 3^\circ$. Moreover, suppose the wheel is travelling at $V_r = 10$ m/s, with $\sigma_x = \sigma_y = 0$. Find the spin slip φ in the following cases:

1. the wheel goes straight ahead;
2. the wheel moves clockwise on a circular path of radius $r_p = 10$ m;
3. as above, but counterclockwise;
4. the wheel moves clockwise on a circular path of radius $r_p = 50$ m.

Solution

Let ω_c be the angular velocity of the rim around its spindle axis. Since $\sigma_x = 0$, in all cases we have $\omega_c = V_r/r_r = 38.2$ rad/s. Moreover, let ω_z be the yaw rate of the rim.

To answer the first question, which requires $\omega_z = 0$, we can use (2.68). The resulting spin slip is $\varphi = -0.1$ m⁻¹.

To answer question number two (Fig. 2.16) we first compute $\omega_z = -V_r/r_p = -10/10 = -1$ rad/s. Then, we can employ (2.65) to get $\varphi \simeq 0$. Therefore, according to (2.70), the tire is in pure rolling conditions.

In the third question we have $\omega_z = 1$ rad/s. Therefore, again from (2.65), we obtain $\varphi = -0.2$ m⁻¹.

In the last problem we have $\omega_z = -V_r/r_p = -10/50 = -0.2$ rad/s. Applying (2.65) we obtain $\varphi = -0.08$ m⁻¹.

Now we can comment on these results. A camber angle $\gamma = 3^\circ$ is quite high for a car tire. The radius of the path $r_p = 10$ m, which is a rather sharp turn, was chosen to get $\varphi \simeq 0$ in question number two. Notably, it is more or less the kind of radius of the FSAE skid-pad event.

In this exercise we have done kinematics of the rigid rim, but taking also into account two features of the tire. Namely, the rolling radius r_r and the camber reduction factor ε_r .

2.15.5 Motorcycle Tire

Let a tire have a rolling radius $r_r = 0.262$ m and a camber reduction factor $\varepsilon_r = 0$. Moreover, suppose the wheel is travelling at $V_r = 10$ m/s, with $\sigma_x = \sigma_y = 0$ and a camber angle $\gamma = 45^\circ$. Find the spin slip φ in the following cases:

1. the wheel goes straight ahead;
2. the wheel moves clockwise on a circular path of radius $r_p = 10$ m.

Solution

Let ω_c be the angular velocity of the rim around its spindle axis. Since $\sigma_x = 0$, in all cases we have $\omega_c = V_r/r_r = 38.2$ rad/s. Moreover, let ω_z be the yaw rate of the wheel.

To answer the first question, which requires $\omega_z = 0$, we can use (2.68). The resulting spin slip is $\varphi = -2.7\text{m}^{-1}$. As expected, the spin slip is very high.

To answer question number two (Fig. 2.16) we compute first $\omega_z = -V_r/r_p = -10/10 = -1$ rad/s. Then, we can employ (2.65) to get $\varphi = -2.6\text{m}^{-1}$. We see that the turn slip contribution to the spin slip is quite small.

To have pure rolling we should have $\omega_z/\omega_c = -\sin(\gamma) = -r_r/r_p = -0.7$. That is a path with radius $r_p = r_r/0.7 = 0.37$ m.

2.15.6 Finding the Magic Formula Coefficients

The results obtained in a purely lateral test on an FSAE tire are shown in Fig. 2.46. This test was conducted with an almost constant vertical load $F_z = 700$ N on a free rolling wheel with zero camber angle. We want to find a fairly good set of Magic Formula coefficients to fit these data.

Solution

The first step is finding the peak value y_m . We see that the positive and negative peak values are not exactly the same. This is quite typical. Setting $D = -y_m = -1100$ N seems a reasonable choice.

Incidentally, we observe that this tire has a global lateral friction coefficient $\mu_p^y = 1100/700 = 1.57$. Not bad.

The second step looks more tricky. We need the asymptotic value y_a , but this value is not readily available from the plot, as tests are carried out up to about $|\sigma_y| = 0.2$,

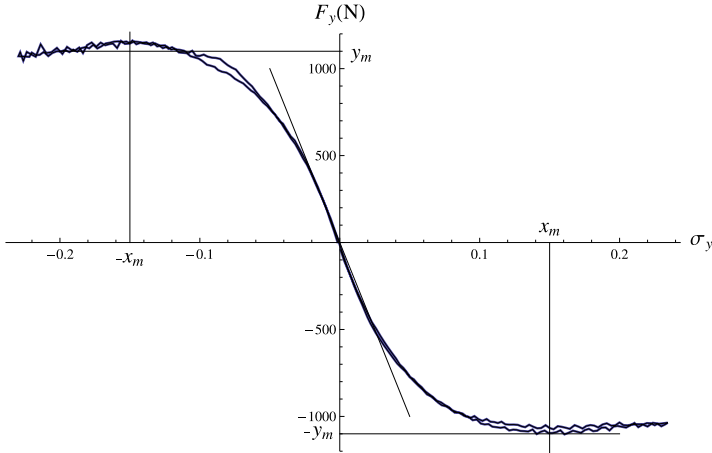


Fig. 2.46 Lateral force F_y due to pure lateral slip σ_y for an FSAE tire

that is $|\alpha| = 12^\circ$, to avoid tire damage. We try $y_a = 800$ N, and, according to (2.96), we get the shape factor coefficient $C = 1.48$.

The third step needs also the slope in the origin. From Fig. 2.46 we obtain $F'_y(0) = -20000$ N, and hence, according to (2.97), $B = 20000/(CD) = 12.27$.

Finally, we see that the peak values are attained for $\sigma_y = x_m = 0.15$. Therefore, according to (2.98) and employing the just found values of C and B , we get the curvature factor $E = 0.07$.

Now we can check whether the Magic Formula with our set of parameters

$$F_y(\sigma_y) = -1100 \sin\left\{1.48 \arctan\left[12.27\sigma_y - 0.07(12.27\sigma_y - \arctan(12.27\sigma_y))\right]\right\} \tag{2.114}$$

provides a good approximation of the experimental data of Fig. 2.46. This is done in Fig. 2.47. We see that, indeed, the smooth curve hits the target.

Actually, we observe that it has been too easy. Indeed, our guess for y_a was not really supported by available data, but nonetheless the final result is very good. Therefore, we repeat the whole procedure, employing the same values of y_m , $F'_y(0)$, and x_m , but with a very different guess about the asymptotic value y_a . For instance $y_a = 550$ N. The resulting new set of parameters is $D = -1100$ N, $C = 1.67$, $B = 10.91$, and $E = 0.41$. As expected, we got very different values.

Let us do it once more, with an unrealistic low value $y_a = 200$ N. After the same steps we get $D = -1100$ N, $C = 1.88$, $B = 9.65$, and $E = 0.72$.

You see, we selected three very different asymptotic values for y_a . Which provided very different values of C , B , and E . But what about their corresponding plots? Surprisingly enough, as shown in Fig. 2.48, they are practically indistinguishable in the range of interest, that is $-0.2 < \sigma_y < 0.2$. Therefore, the selection of y_a is not tricky at all, contrary to our first impression. Much more important are the other three conditions on y_m , $F'_y(0)$, and x_m . Indeed, requiring a function to start with a given

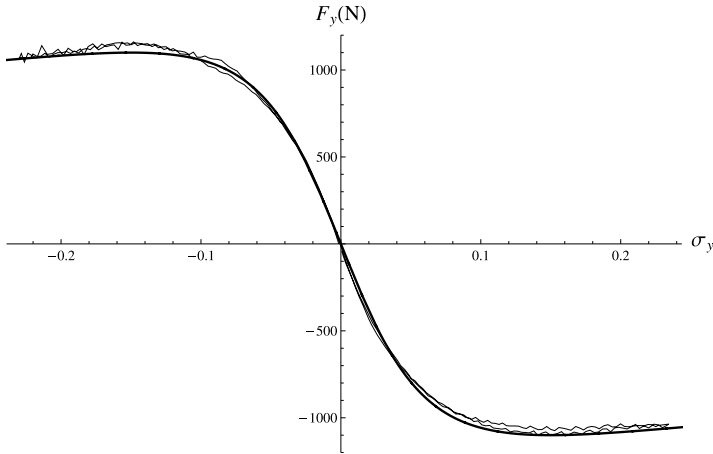


Fig. 2.47 Experimental tire data and Magic Formula fitting

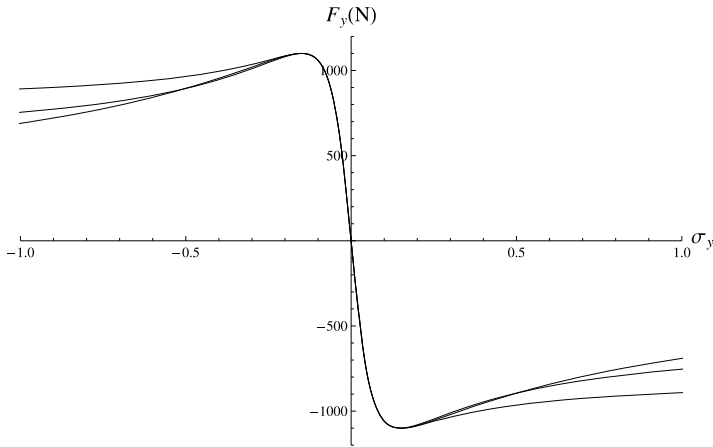


Fig. 2.48 Comparison of three Magic Formula fittings with different y_a

slope at the origin, and then to reach a maximum at a given point does not leave much room.

These results may have relevant practical implications: the very same tire behavior can be associated to very different sets (C, B, E) of three out of four Magic Formula parameters. For instance, in our case, the three sets of the coefficients (C, B, E)

- (1.48, 12.27, 0.07);
- (1.67, 10.91, 0.41);
- (1.88, 9.65, 0.72);

are pretty much equivalent in the range of interest for σ_y (Fig. 2.48). Therefore, looking at the MF parameters may not be a good way to promptly understand the

mechanical behavior of a wheel with tire. It is somehow an ill-conditioned problem. More precisely, the final MF fitting plot is almost insensitive to the asymptotic value y_a , at least for $0.2 < y_a/y_m < 0.85$, whereas (C, B, E) change a lot.

From another point of view, in most cases we can select y_a in such a way to have $E = 0$, thus simplifying the Magic Formula, but still with a very good fitting.

2.16 Summary

In this chapter we have first pursued the goal of clearly describing the relevant kinematics of a wheel with tire, mainly under steady-state conditions. This had led to the definitions of slips as a measure of the extent to which the wheel with tire departs from pure rolling conditions. The slip angle has been also defined and discussed. It has been shown that a wheel with tire resembles indeed a rigid wheel because slip angles are quite small. Tire experimental tests show the relationships between the kinematics and the forces/couples the tire exchanges with the road. The Magic Formula provides a convenient way to represent these functions. Finally, the mechanics of the wheel with tire has been summarized with the aid of a number of plots.

2.17 List of Some Relevant Concepts

Section 2.1 a wheel with tire is barely a wheel;

Section 2.4.2 there are two distinct contributions to the spin velocity of the rim;

Section 2.4.2 in a wheel, longitudinal velocities are expected to be much higher than lateral ones;

Section 2.5.1 the name “self-aligning torque” is meaningless and even misleading;

Section 2.6.3.1 rim kinematics depends on six variables, but often (not always) only five may be relevant for the tire;

Section 2.7 a reasonable definition of pure rolling for a wheel with tire is that the grip local actions have no global effect;

Section 2.8 tire slips measure the distance from pure rolling;

Section 2.8.5 tire slips do not provide any direct information on the amount of sliding at any point of the contact patch;

Section 2.10 tire forces and moments depend on both the camber angle and the spin slip;

Section 2.12.6 pure rolling and free rolling are different concepts.

2.18 Key Symbols

a	drive lever arm
B	stiffness factor
C	point of virtual contact
C	shape factor
c_r	distance OC
D	peak value
E	curvature factor
F_x	longitudinal force
F_y	lateral force
F_z	vertical force
h	height above ground of the center of the rim
M_x	overturning moment
M_y	rolling resistance moment
M_z	vertical moment
O	center of the footprint
r_r	rolling radius
\mathbf{V}_c	travel velocity
V_{ox}	longitudinal velocity of O
V_{oy}	lateral velocity of O
V_r	rolling velocity
\mathbf{V}_s	slip velocity
α	slip angle
γ	camber angle
ε_r	camber reduction factor
μ_p^x	longitudinal friction coefficient
μ_p^y	lateral friction coefficient
σ_x	longitudinal slip
σ_y	lateral slip
φ	spin slip
ω_c	angular velocity of the rim around its axis
ω_r	rolling yaw rate of the reference system
ω_z	yaw rate of the reference system

References

1. Bakker E, Pacejka H, Lidner L (1987) Tyre modelling for use in vehicle dynamics studies. SAE Trans 96:190–204
2. Bakker E, Pacejka H, Lidner L (1989) A new tire model with an application in vehicle dynamics studies. SAE Trans 98:101–113

3. Bastow D, Howard G, Whitehead JP (2004) Car suspension and handling, 4th edn. SAE International, Warrendale
4. Bergman W (1977) Critical review of the state-of-the-art in the tire and force measurements. SAE Trans 86:1436–1450
5. Clark SK (2008) The pneumatic tire. NHTSA-DOT HS 810 561
6. Dixon JC (1991) Tyres, suspension and handling. Cambridge University Press, Cambridge
7. Font Mezquita J, Dols Ruiz JF (2006) La Dinámica del Automóvil. Editorial de la UPV, Valencia
8. Gillespie TD (1992) Fundamentals of vehicle dynamics. SAE International, Warrendale
9. Jazar RN (2017) Vehicle dynamics, 3rd edn. Springer, New York
10. Johnson KL (1985) Contact mechanics. Cambridge University Press, Cambridge
11. Leneman F, Schmeitz A (2008) MF-Tyre/MF-Swift 6.1.1. TNO Automotive, Helmond
12. Meirovitch L (1970) Methods of analytical dynamics. McGraw-Hill, New York
13. Michelin (2001) The tyre encyclopaedia. Part 1: grip. Société de Technologie Michelin, Clermont–Ferrand, [CD-ROM]
14. Michelin (2002) The tyre encyclopaedia. Part 2: comfort. Société de Technologie Michelin, Clermont–Ferrand, [CD-ROM]
15. Michelin (2003) The tyre encyclopaedia. Part 3: rolling resistance. Société de Technologie Michelin, Clermont–Ferrand, [CD-ROM]
16. Milliken WF, Milliken DL (1995) Race car vehicle dynamics. SAE International, Warrendale
17. Murray RM, Li Z, Sastry SS (1994) A mathematical introduction to robot manipulation. CRC Press, Boca Raton
18. NHTSA (2009) The effects of varying the levels of nitrogen in the inflation gas of tires on laboratory test performance. Report DOT HS 811 094, National Highway Traffic Safety Administration, Washington
19. Pacejka HB (1996) The tyre as a vehicle component. In: 26th FISITA congress '96: engineering challenge human friendly vehicles, Prague, June 17–21, pp 1–19
20. Pacejka HB (2002) Tyre and vehicle dynamics. Butterworth-Heinemann, Oxford
21. Pacejka HB (2005) Slip: camber and turning. Veh Syst Dyn 43(Supplement):3–17
22. Pacejka HB (2012) Tire and vehicle dynamics, 3rd edn. Butterworth-Heinemann, Oxford
23. Pacejka HB, Bakker E (1992) The magic formula tyre model. Veh Syst Dyn 21:1–18. <https://doi.org/10.1080/00423119208969994>
24. Pacejka HB, Sharp RS (1991) Shear force development by pneumatic tyres in steady state conditions: a review of modelling aspects. Veh Syst Dyn 20:121–176
25. Popov VL (2010) Contact mechanics and friction. Springer, Berlin
26. Purdy JF (1963) Mathematics underlying the design of pneumatic tires. Edwards Brothers, Ann Arbor
27. Pytel A, Kiusalaas J (1999) Engineering mechanics-statics. Brooks/Cole, Pacific Grove
28. Schramm D, Hiller M, Bardini R (2014) Vehicle dynamics. Springer, Berlin
29. Seward D (2014) Race car design. Palgrave, London
30. Wong JY (2001) Theory of ground vehicles. Wiley, New York
31. Wright C (2013) The contact patch. <http://the-contact-patch.com/book/road/c1610-rubber-tyres>
32. Zegelaar P (1998) The dynamic response of tyres to brake torque variations and road unevennesses. Delft University of Technology, Delft